R. & M. No. 3626

R. & M. No. 3626

MINISTRY OF TECHNOLOGY

AERONAUTICAL RESEARCH COUNCIL
REPORTS AND MEMORANDA

Pressure Measurements on a Slender Rhombic Cone at Incidence at Mach Numbers from 0·4 to 1·1

By J. H. B. SMITH and A. G. KURN
Aerodynamics Dept., R.A.E., Farnborough

LONDON: HER MAJESTY'S STATIONERY OFFICE
1970
PRICE 19*s* 0*d* [95*p*] NET

Pressure Measurements on a Slender Rhombic Cone at Incidence at Mach Numbers from 0·4 to 1·1

By J. H. B. SMITH and A. G. KURN

Aerodynamics Dept., R.A.E., Farnborough

Reports and Memoranda No. 3626*

July, 1968

Summary.

Pressures have been measured on a wing in the form of a rhombic cone at two cross-sections and along a single generator. The wing had an aspect ratio of one and a leading-edge angle of 60°. Measurements were made at $M = 0{\cdot}4, 0{\cdot}6, 0{\cdot}82, 0{\cdot}9, 1{\cdot}0$ and $1{\cdot}1$, at angles of incidence up to 20° and at a Reynolds number of 6 million, based on model length. At the lowest Mach number the tests were repeated at higher Reynolds number.

The measured pressure distributions are typical of flow with leading-edge vortices. Two different types of suction peaks were observed and associated, on indirect evidence, with the state of the boundary layer at secondary separation. Within each type, increasing Mach number reduced the magnitude of the peak suction, but had little effect on its spanwise location. At transonic and high subsonic speeds an increase in incidence above 8° changed the shape of the suction peak from the type associated with a turbulent secondary separation to that associated with a laminar one.

LIST OF CONTENTS

*Replaces R.A.E. Technical Report 68 171—A.R.C. 30 735

LIST OF CONTENTS—*continued*

---

1. *Introduction.*

It is well known (*see* Küchemann[1], for example) that the peak suction on the upper surface of a slender wing under a leading-edge vortex is much lower at supersonic speeds that at low subsonic speeds, for the same incidence. At higher supersonic speeds the peak suction is still lower. It is also familiar (Squire and Capps[2], Squire[3]) that both the linear part of the lift and the non-linear part of the lift, which is associated with the presence of leading-edge vortices, increase as the Mach number rises towards one and then fall off with further increase in Mach number. However, the variation with Mach number of the pressure distribution in the presence of leading-edge vortices at subsonic and transonic speeds has not previously been examined.

Apart from its intrinsic interest, the transonic flow past a slender wing is relevant to any discussion of the attempts that have been made to calculate the flow with leading-edge separation, because many of these, including the currently most sophisticated (Smith[4]), make use of slender-body theory, and this theory is expected to be most accurate in its prediction of lifting effects at transonic speeds. Since there are significant differences between theory and observations made at low speeds, there is interest in whether these differences are reduced at transonic speeds or whether the deficiency lies in the vortex-sheet model rather than in the use of slender-body theory to calculate its properties.

To provide some information on the development of the separated flow with Mach number, an existing model used by Britton[5] in the 8 ft × 8 ft supersonic tunnel at R.A.E. Bedford was tested in the 8 ft × 6 ft transonic tunnel at R.A.E. Farnborough. This was a delta wing of aspect ratio one, in the form of a cone of rhombic cross-section, the interior angle of the cross-section at the leading-edge being 60° (*see* Fig. 1). A comprehensive set of pressure measurements was made on a cross-section 33·6 per cent of the model length from the apex and along a generator at 59·7 per cent of the local semi-span from the centreline. The measurements at these positions raised additional questions which were largely resolved by supplementary

measurements on a cross-section at 60·1 per cent of the length from the apex, and by repeating a few critical cases with roughness bands to promote transition in the boundary layer flowing outboard under the vortex.

It is possible to regard this boundary layer as originating at an attachment line on the upper surface of the wing, somewhat inboard of the vortex. From this line the boundary layer is swept outboard under the vortex, initially in a region of rapidly falling pressure; then, passing beneath the vortex, it encounters a rising pressure and eventually separates. With a turbulent boundary layer this separation occurs closer to the leading edge than with a laminar layer. This behaviour is clearly shown in photographs of surface oil-flow by Hummel[6] and measurements of surface pressure by Gregory and Love[7]. The suction peak associated with turbulent secondary separation is typically sharper, higher, and somewhat further outboard, than that measured when the boundary layer is still laminar at separation. (*See*, for instance, the results collected by Smith[4].) There is also a substantial recompression between the vortex and the leading edge in the turbulent case.

Suction peaks of both types were observed at the forward measuring station in the present experiments. The broad, inboard peak associated with laminar separation was found only at low incidence ($\alpha \leqslant 4°$) and when both the Mach number and the incidence were high; $M \geqslant 0{\cdot}82$ and $\alpha \geqslant 12°$. In the supplementary tests, at high Mach number and incidence, no peaks of this kind were observed at the aft station. When the model was roughened with carborundum grains on the apex and along part of a generator between the attachment line and the suction peak, no peaks of the laminar type were observed at either cross-section at high Mach number and incidence.

At subsonic speeds even the inviscid flow over a conical body is not conical, that is to say the velocity is not constant along rays through the apex. However, much of the deviation from conicality, particularly towards the apex of the body, arises from the displacement flow. If the pressures measured at zero incidence are subtracted from those measured at a given non-zero incidence, the 'lifting pressure field' which results is more nearly conical, although the loading must still fall to zero at the trailing edge. This procedure is discussed in the context of slender-body theory in Appendix A and shown to be meaningful, except for large incidences at transonic speeds. The present measurements show that, when the suction peak at the forward measuring station is of the turbulent type, substantially the same lifting pressure field is found at the forward and aft stations, and the lifting pressure is constant over the middle part of the body length along the generator on which measurements were made. When the Mach number and incidence were high, and transition was not artificially induced, the lifting pressure field was markedly non-conical.

The interpretation of the variation of the magnitude and position of the suction peak with Mach number and incidence is complicated by the change in character of the peak. In general the peak suction for a given incidence falls with increasing Mach number, the values for $0{\cdot}4 \leqslant M \leqslant 1{\cdot}1$ from the present tests joining more or less continuously to those of Britton[5] for $M \geqslant 1{\cdot}3$. The fall through the transonic range, $0{\cdot}9 \leqslant M \leqslant 1{\cdot}1$, is very rapid at high incidence, but at $\alpha = 4°$ the variation is insignificant. Such a reduction in peak suction is not, of course, inconsistent with the observed increase in overall lift as the Mach number rises towards one. Not only is there some increase in lower surface pressure noticeable at the forward station, but the loading is carried progressively closer to the trailing edge as the Mach number rises subsonically. The changes in position of the suction peak with Mach number are very small, unless the peak changes character. Such changes as there are within each family of peaks are consistent with a slight inboard movement of the vortex as the Mach number rises. This is the direction of the change which has been noted by Gaudet and Winter[8] between low speed and supersonic observations. The variation with incidence at each Mach number is similar to that familiar from low speed experiments, provided the character of the peak is unchanged. As the incidence increases, the peak intensifies, widens and moves inboard.

The most surprising outcome of the experiment is in relation to the variation with incidence of the Reynolds number for transition in the boundary layer under the vortex. Although no direct observations of the boundary layer were made, the circumstantial evidence associating the observed types of suction peak with different states of the boundary layer is strong. If this is accepted, then the results show that at high subsonic and transonic Mach numbers an increase in incidence produces an increases in this transition Reynolds number. This is the opposite trend to that observed at low subsonic speeds.

It is possible to suggest how this might come about, though in the absence of observations of either the flow field or the boundary layer such an explanation must be tentative in the extreme. There is some evidence (*see* Gaudet and Winter[8]) that, at a fixed angle of incidence, the leading-edge vortex moves closer to the plane of the wing as Mach number increases. This may well mean that the secondary boundary layer under the vortex is thinner and more strongly accelerated at the high Mach numbers, so that transition is delayed to a higher Reynolds number. If the movement noted by Gaudet and Winter between low speeds and supersonic speeds is already occurring at the subsonic and transonic speeds of the present tests, this would explain the rise in transition Reynolds number with Mach number at high incidence which is implied by the present measurements.

2. *Experimental Details.*

2.1. *The Model.*

The model, shown in Figs. 1 and 2, was a delta wing of aspect ratio one in the form of conical body with a rhombic cross-section. The interior angle of the rhombus at the leading edge was 60°. The model was 33 inches long and 16·5 inches in span.

Static-pressure holes were situated in three rows (*see* Fig. 1). One row lay along a generator of the conical body at 59·7 per cent of the semi-span from the centreline, on the port upper surface. The other two rows were at lengthwise stations of 33·6 and 60·1 per cent of the length from the apex on the upper and lower surfaces of the starboard side, respectively. The locations of the holes in the rows are given in Table 2.

2.2. *Range of Investigation.*

Pressure measurements were made in the R.A.E. 8 ft × 6 ft transonic wind tunnel, with the model supported from its base by a sting, as shown in Fig. 2. For the main series of tests, before the aft station was instrumented, the incidence range was from $-4°$ by 2° to 8° and then by 4° to 20° at Mach numbers of 0·40, 0·60, 0·82, 0·90, 1·00 and 1·10. At the lowest Mach number, measurements were made at Reynolds numbers of 2, 4 and 6 million per foot; at the higher Mach numbers measurements were confined to the lowest Reynolds number. Since the model was instrumented on one surface only at each of the measuring stations, pressure readings appropriate to the opposite surface were obtained by repeating each run with the model rolled through 180°. The aft row of pressure holes was fitted for supplementary tests at $\alpha = 0°$, 8° and 16° at particular Mach numbers.

2.3. *Transition Fixing.*

Some runs were repeated with the model surface roughened locally with carborundum particles. The grain size was 60–52, meaning that the particles passed through a sieve with 0·0110 inch holes, but were retained in a sieve with 0·0099 inch holes. The particles were applied uniformly over the first 5 per cent of the model length, except that the leading edges were kept clean. In addition, strips of a width equal to 5 per cent of the local semi-span were applied between suitably chosen generators, starting from the roughened nose and stopping short of the spanwise rows of pressure holes. For the measurements at an incidence of 8° ($M = 0·40$, 0·60 and 0·82), the strips lay between 67·5 and 72·5 per cent of the semi-span and stopped 0·5 inch short of the holes. At an incidence of 16° ($M = 0·82$ and 0·90), the strips lay between 50 and 55 per cent of the semi-span and stopped 1 inch short of the forward holes and 2 inches short of the rearward holes. In each case, the position of the roughness strip was chosen to lie outboard of the main attachment line on the upper surface and inboard of the secondary separation line.

2.4. *Incidence Correction.*

No incidence correction has been applied. There are two possible sources of error: the deflection of the model and its support under load, and the interference of the tunnel walls.

The model and its support are massive, as can be seen in Fig. 2. At the lowest Mach number of the tests ($M = 0·4$), the Reynolds number was increased by a factor of 3, corresponding to threefold increase in the aerodynamic loading. As discussed in Section 3.2, there was no effect on the surface pressure coefficient which could be attributed to a change in the incidence of the model. The dynamic pressure

in the remaining tests at constant Reynolds number was proportional to the Mach number and so increased rather less than threefold over the range $0{\cdot}4 \leqslant M \leqslant 1{\cdot}1$. It is unlikely that significant deflection occurred.

The calculation of wall interference for transonic flow in a tunnel with slotted walls is difficult. To estimate the order of the incidence correction, the method of Berndt[9] has been applied to calculate the correction which would be appropriate for incompressible flow in a tunnel with solid walls. According to this method, the incidence correction varies along the length of the model. At the forward station we find

$$\Delta\alpha = 0{\cdot}0035\, C_L .$$

For a delta wing of unit aspect ratio at low speeds, Earnshaw and Lawford[10] find $C_L = 0{\cdot}67$ for the mean lift coefficient of their slightly cambered model at $\alpha = \pm 20°$. With the formula above this gives $\Delta\alpha < 0{\cdot}14°$, which can be ignored for the present investigation. As the Mach number increases towards unity the incidence correction for a solid-wall tunnel tends to infinity. On the other hand, for an ideal ratio of the areas of slot and solid wall, the interference in a slotted-wall tunnel can be zero. In these circumstances it did not appear worthwhile to try to correct for wall interference.

2.5. *Blockage Correction.*

No blockage correction has been applied, partly because of uncertainty about how it should be calculated and partly because of indications that blockage effects do not affect the interpretation of the results.

For bluff-based slender models of this kind in rectangular, solid-wall tunnels in essentially incompressible flow, Kirkpatrick[11] has proposed a method of calculating the blockage correction directly from the model shape. His method is summarised in Appendix B. For the present case we find proportional increases in streamwise velocity, $\Delta U/U$, of 0·0047 at the forward measuring station and 0·0055 at the aft station. These are so small that we feel justified in neglecting blockage corrections at the lower Mach numbers.

As an indication of the magnitude of the blockage effect in a slotted-wall tunnel at transonic speeds, we quote a result derived by Berndt[12]. This assumes disturbances much smaller than those of the present tests, treats a body of revolution in a circular working section and involves a number of approximations. The result is that to reproduce sonic speed in the working section the upstream Mach number is $1 - \Delta M_0$, where

$$\Delta M_0 = 0{\cdot}9\, g \left(\frac{\tau l}{R}\right)^{6/7} \tau^{2/7} .$$

Here $g = 0{\cdot}292$ for an optimised slot geometry, τ is the thickness ratio, l is the body length and R is the radius of the test section. Writing $\tau^2 = B/\pi l^2$, where B is the base area of the model, and $\pi R^2 = \lambda b^2$, where b is the tunnel breadth and λb the tunnel height, we find $\Delta M_0 \simeq 0{\cdot}02$. This is certainly not negligible; but the applicability of Berndt's analysis to the present case is so uncertain and the conclusions drawn from the present tests depend so little on precise values of Mach number that no advantage is seen in applying the correction.

2.6. *Reduction of Pressure to Coefficient Form.*

The pressures, measured on self-balancing capsule manometers, were reduced to pressure coefficient form by the standard method used in the 8 ft × 6 ft transonic tunnel.

Briefly, the tunnel speed and total pressure are monitored from pressures measured in the settling chamber and in the plenum chamber surrounding the slotted working section. Corrections to these pressures, to obtain those appropriate to an empty working section, are obtained from a tunnel calibration and fed into a computer programme which calculates pressure coefficients from the pressures measured on the model.

3. *Results.*

3.1. *Earlier Work on the Effect of the State of the Secondary Boundary Layer.*

The air flowing outboard over the upper surface of the wing, beneath the vortex which springs from the leading edge, forms a boundary layer which we can call the secondary boundary layer. As this flow passes beneath the vortex, it encounters a rising pressure and the secondary boundary layer separates. The lateral position of this secondary separation line depends on whether the boundary layer is laminar or turbulent, as shown by Lawford[13]. The influence of this on the position of the primary vortex, the pressure distribution on the wing and the overall lift were discussed by Smith[4]. Briefly, measurements by Gregory and Love[7] show a change in the character of the main suction peak on the upper surface: when the secondary boundary layer is turbulent at separation the peak is higher, sharper and slightly further outboard than when the boundary layer remains laminar up to separation.

At low speeds, on a wing of a particular aspect ratio, Hummel[6] showed that the Reynolds number based on the distance from the apex of the wing to the lengthwise station at which transition occurs in the secondary boundary layer depended only on incidence. The dependence which he found is shown in Fig. 3. Gregory and Love[7] found a much slower variation with incidence, the curve shown in Fig. 3 representing the maximum variation found in their experiments. As would be expected, in a different tunnel the level of Reynolds number is different. Lemaire[14] presented a large number of pressure measurements, again on a delta wing of aspect ratio one, at various Reynolds numbers. She did not relate the change in suction peak shape to a change in the state of the secondary boundary layer, but a classification of the peak shapes she observed on the qualitative basis mentioned above leads to the curve shown in Fig. 3. The resemblance between this curve and that of Hummel supports the belief that the shape of the suction peak can be a useful guide to the state of the secondary boundary layer.

3.2. *Variation of Reynolds Number.*

At the lowest Mach number of the tests ($M = 0{\cdot}4$) it was possible to increase the Reynolds number from the standard 2 million per foot to 4 and 6 million per foot. The distribution of pressure coefficient at the forward station at these three Reynolds numbers, with free transition, is shown in Figs. 4a and 4b for 8° and 16° incidence. The increase in Reynolds number is accompanied by an increase in tunnel pressure, so that, in addition to aerodynamic effects, it increases the manometer deflections, making the determination of C_p more accurate, and it may produce distortion of the model or its support.

The first point to be made about Fig. 4 is that the shapes of the suction peaks are substantially unaffected by the change of Reynolds number. Since the secondary separation at the highest Reynolds number would undoubtedly by turbulent according to Fig. 3, we conclude that it is also turbulent at the lowest Reynolds number, at which the remainder of the measurements were made. A turbulent secondary separation at Reynolds numbers of 2 million and above, at incidences of 8° and above, is consistent with Fig. 3, if the turbulence level in the present tunnel is rather higher than that of the N.P.L. tunnel used by Gregory and Love[6]. The suction peaks shown in Fig. 4, with substantial recompression between the position of minimum pressure and the leading edge, are typical of turbulent secondary separation.

Considering now the small differences between the results for different Reynolds numbers, we find it convenient to examine separately the lower surface, the inboard part of the upper surface, the main suction peak and the region of secondary separation. On the lower surface there is apparently a small increase in pressure coefficient with Reynolds number, except close to the leading edge. When the pressure coefficient at zero incidence is subtracted to give the 'lifting pressure field' (*see* Appendix A), no systematic effect of Reynolds number remains, except that near the leading edge the lifting pressure coefficient goes down slightly as Reynolds number rises. Since the primary attachment line moves from the leading edge to the lower surface at positive incidence, the boundary layer near the leading edge may well be thinner at positive incidence than at zero incidence. This suggests that the effect of Reynolds number on the lower-surface pressures may be a boundary-layer effect, but no quantitative estimate is possible in the absence of transition observations. Most of the results are presented in terms of lifting pressures, where the variation with Reynolds number is much smaller.

On the inboard part of the upper surface there is no systematic effect of Reynolds number noticeable

in Fig. 4. Near the peak suction, the pressure gradients are large and it appears that small changes in the position of the vortex have given rise to quite marked differences in pressure coefficient between one Reynolds number and another. No importance is attached to these, since slight variations in vortex position, up to about 2 per cent semi-span, may arise from the non-conicality of the flow with free transition in the secondary boundary layer. In the region of secondary separation, the increase in Reynolds number seems to result in an increased suction. At the higher incidence, Fig. 4b, this produces a well-defined secondary peak.

In view of the above discussion, it is concluded that there is no evidence of significant distortion of the model or its support at the highest Reynolds number of the tests. Fig. 4 shows that, as expected, the scatter between measurements at adjacent holes is reduced as the Reynolds number increases. The scatter is still significant at 6 million and disturbingly large at 2 million, since this is the Reynolds number of the remaining tests. However, at the higher Mach numbers the dynamic pressure is higher and smoother curves are obtained. Some further alleviation occurs when the lifting pressure is calculated, because some errors seem to be associated, more or less permanently, with particular static holes or the manometers to which they are connected. Similar 'bumps' can be seen in the upper and lower surface distributions in Fig. 4 and they appear also in the zero incidence distributions (*see* Fig. 5). Indirect evidence suggesting the static holes are at fault comes from Fig. 7, where measurements at the newly-fitted holes at the aft station are smoother than those at the forward station.

3.3. *Variation of Incidence.*

In Fig. 5, the distribution of pressure coefficient across the semi-span is shown for $\alpha = 0°, 4°, 8°, 12°, 16°$ and $20°$ at $M = 0{\cdot}6$, 0·82 and 1. In general terms, the development with incidence is that familiar from earlier tests at lower and higher Mach numbers. On the centreline, increasing incidence causes roughly proportional increases in suction on the upper surface and pressure on the lower surface. Outboard on the upper surface the suction peak under the vortex grows in height and breadth and moves inboard, leaving an increasing area of roughly constant pressure between it and the leading edge. The lower surface pressures near the leading edge are reduced towards the low pressure on the upper surface.

Looking more closely at the development of the suction peak with incidence we see changes in its character. The results shown in Fig. 5 were obtained with free transition, at a Reynolds number based on the distance to the measuring station of 2 million, so examples of both laminar and turbulent secondary separation may be expected. In Fig. 5a, for $M = 0{\cdot}6$, the peak at $\alpha = 4°$ appears to correspond to a laminar separation, while those at the higher incidences are typical of turbulent separation. Transition between $\alpha = 4°$ and $8°$ at $Re = 2 \times 10^6$ is consistent with Fig. 3, which was constructed for Mach numbers less than 0·2. In Fig. 5b, for $M = 0{\cdot}82$, it again appears that the peak at $\alpha = 4°$ correponds to a laminar separation and that at $\alpha = 8°$ to a turbulent one. However, at the higher incidences the position is not so clear. At $\alpha = 16°$ the shape of the suction peak is typical of laminar secondary separation, while those at $\alpha = 12°$ and $20°$ may be intermediate in character, perhaps associated with a non-conical flow due to the proximity of the transition region. In Fig. 5c, for $M = 1$, the peaks at $\alpha = 4°$ and $16°$ are again of the laminar type. The pressure recoveries between the vortex and the leading edge at the other incidences are smaller than at the lower Mach number, so that $\alpha = 12°$ and $20°$ also seem to be laminar, though $\alpha = 8°$ is possibly still turbulent. This discussion will be resumed later in relation to the other figures, but it already seems likely that the variation of Reynolds number for transition in the secondary boundary layer becomes more complex at the higher Mach numbers.

The critical level of C_p, at which the speed becomes sonic, is shown in Fig. 5b. It is of no particular significance in this nearly conical flow; the more significant quantity, the Mach number of the component of velocity normal to the conical ray, can only be determined when the flow direction is known. This question is discussed towards the end of Section 3·5.

At the two highest incidences in Figs. 5b and 5c there are three separate humps on the suction peak. It would be reasonable to associate these with the primary, secondary and tertiary vortices were it not that the smallest hump disappears when the zero incidence pressures are subtracted, as is apparent in Figs. 8a and 8b.

3.4. *Conicality of the Flow and the Effect of Roughness.*

The subsonic and transonic flow past a slender conical body is not conical, that is to say the velocity and pressure vary along rays through the apex of the body. However, if the displacement flow of the body is subtracted, the resulting flow field due to lift is more nearly conical. Appendix A shows that, in particular, the lifting pressure as calculated by slender body theory is conical. In practice the lifting pressure field will depart from conicality near the apex, where the disturbances are not small, and near the trailing edge, where the Kutta condition must be satisfied.

In the present series of measurements two tests of the conicality of the lifting pressures are possible. We can examine the variation of lifting pressure along the ray at 60 per cent of the local semi-span and we can compare the measurements at the forward (34 per cent) and aft (60 per cent) stations for those cases for which the aft station was instrumented. The pressures along the ray are a particularly sensitive indication of the conicality of the flow when the suction peak lies over the ray.

At 4° and 8° incidence the suction peak is outboard of the 60 per cent ray at all Mach numbers. There is no significant variation of lifting pressure between 10 and 90 per cent of the model length for $\alpha = 4°$ and between 10 and 80 per cent for $\alpha = 8°$. Further forward the lifting pressure on the upper surface is a little more negative, and further aft it increases towards zero if $M < 1$. For $M \geqslant 1$ there is no significant loss of lifting pressure towards the trailing edge up to 90 per cent of the model length at any incidence. At 12° incidence the 60 per cent ray lies on the inboard slope of the suction peak at all Mach numbers and, for $M < 1$, the lifting pressure on the upper surface rises towards zero along the ray from 5 to 90 per cent of the length. The rise is steepest near the apex and the trailing edge, but amounts to about $\Delta C_{p_L} = 0{\cdot}15$ between 20 and 80 per cent of the length. These results are not reproduced in detail in the Report.

Fig. 6a shows the distribution of lifting pressure coefficient at $\alpha = 16°$ along the 60 per cent ray on the upper surface. At this incidence the suction peak is over the ray and we have a sensitive test of the conicality of the flow. Ignoring what happens very close to the apex, we see that at each Mach number the lifting pressure becomes more negative as we go aft, and then the lifting pressure rises towards zero at the subsonic Mach numbers. The lengthwise stations at which the suction intensifies is further aft the higher the Mach number and the suction is maintained closer to the trailing edge the higher the subsonic Mach number.

The relation between this behaviour and the state of the secondary boundary layer is brought out in Fig. 6b. One of the broken lines is taken from Fig. 6a for $M = 0{\cdot}82$, the other is the corresponding curve for $M = 0{\cdot}9$. These are similar over the forward part of the model but reach different levels over the aft part. They are to be compared with the full lines, which represent measurements made with the model roughened as described in 2.3. Very near the apex the measurements seem to have been adversely affected by the proximity of the roughness grains, but it is clear that the roughness has moved the station at which the suction intensifies forward by some 20 per cent of the model length. The close agreement between the free and fixed transition curves further aft is striking. It is concluded that the increase in intensity of the suction peak is due to transition in the secondary boundary layer. We note that, at the forward station at $\alpha = 16°$, the secondary separation is already turbulent at $M = 0{\cdot}4$ and $0{\cdot}6$ on the smooth model, but it is still laminar at $M = 0{\cdot}82$, $0{\cdot}9$ and $1{\cdot}0$, in agreement with the comments made in Section 3.3 on Figs. 4 and 5.

The other evidence on conicality comes from a comparison of results at the forward and aft measuring stations, and again the effect of roughness is relevant. In Fig. 7a the lifting pressure coefficient for $\alpha = 8°$, $M = 0{\cdot}6$ is shown at the forward and aft stations, with and without roughness. Because the distributions are so similar, the curves have been separated by an interval $\Delta C_{p_L} = 0{\cdot}025$. There is no significant effect of roughness and the character of the suction peak is clearly the same at the forward and aft stations, confirming the previous association of this peak with a turbulent secondary separation. Two differences between the forward and aft stations can be seen: the suction peak under the secondary vortex is only evident at the forward station and the position of the minimum pressure under the primary vortex is about 2 per cent of the semi-span further outboard at the aft station. This last feature is also apparent in Fig. 7b, comparing the two curves for the rough model. It is also consistent with the rise in pressure

along the 60 per cent ray mentioned above for $\alpha = 12°$. Such an outward movement of the suction peak between 30 per cent and 60 per cent of the length is not incompatible with an inboard movement of the vortex nearer the trailing edge of the wing, such as has frequently been observed at low speeds.

The principal feature of Fig. 7b, for $\alpha = 16°$ at $M = 0{\cdot}9$, is the non-conicality of the flow on the smooth model and the close approach to conicality when roughness is added. The curves have been separated by $\Delta C_{p_L} = 0{\cdot}05$ for clarity. There is very little effect of roughness at the aft station, which extends the conclusion drawn from Fig. 6b to the whole span and confirms the association of this peak with a turbulent boundary layer. The peak at the forward station is quite different from that at the aft station on the smooth model, but remarkably similar when roughness is added. This also expands the comparison of Fig. 6b and confirms that such broad peaks with little recompression correspond to laminar separation.

The two parts of Fig. 7 are taken to demonstrate conclusively that free transition of the secondary boundary layer occurs further forward at $\alpha = 8°$, $M = 0{\cdot}6$ than at $\alpha = 16°$, $M = 0{\cdot}9$.

3.5. *Variation with Mach Number.*

The discussion of the results so far has been devoted to establishing the significance of the bulk of the measurements, which were taken on the smooth model at the forward station, and to the indirect elucidation of the pattern of transition in the secondary boundary layer. It is clear from this discussion that, at incidences above 8°, the effect of Mach number on the surface pressure distribution is confused by the effect of transition. Nonetheless, it is possible to draw some conclusions from the results, which have been plotted to bring out the effects of Mach number in Fig. 8.

It is convenient to begin with the highest incidence, at which the main features of the lifting pressure distribution are most apparent. Fig. 8a shows the results for $\alpha = 20°$, with the upper and lower-surface distributions on different axes. The lower-surface pressure increases appreciably with Mach number, but the shape of the distribution is unchanged. On the centreline of the upper surface the lifting pressure is unchanged between Mach number 0·4 and 1·0, but then rises between 1·0 and 1·1. The suction peak is plainly of the type associated with a turbulent secondary separation at $M = 0{\cdot}4$ and 0·6 and plainly of the laminar type at $M = 1{\cdot}1$. The peaks at the intermediate Mach numbers have intermediate forms. This is not surprising, since the flow is likely to be unsteady in the neighbourhood of the transition region and neither the average of the unsteady pressures nor steady pressures if they occur are likely to be even approximately conical. There is already an appreciable reduction in peak suction between $M = 0{\cdot}4$ and 0·6, where both peaks are turbulent. Moreover, it seems likely that the sustained reduction in peak suction between $M = 0{\cdot}82$ and 1·1 is due more to the increase in Mach number than to the gradual downstream progress of the transition front. The lateral position of the maximum suction, which indicates the lateral position of the vortex, moves inboard with increase in Mach number. Most of this seems to occur between $M = 0{\cdot}6$ and 0·82, so it is more likely to be a result of the forward movement of the transition than a direct effect of Mach number on the flow outside the boundary layer. This view is supported by Fig. 7b, in which, at the forward station, an outboard shift of the suction peak is shown to correspond to artificially induced turbulence.

At $\alpha = 16°$, Fig. 8b, the variation with Mach number of the lifting pressure on the lower surface and the inboard part of the upper surface are the same as at $\alpha = 20°$. However, it is now possible to associate the suction peaks at $M \geqslant 0{\cdot}9$ with laminar secondary separation, leaving only $M = 0{\cdot}82$ as an intermediate case between these and the peaks of turbulent type at $M = 0{\cdot}4$ and 0·6. It is now clear that the peak suction decreases within each family of suction peaks as the Mach number increases. Results from Britton[5] are included in Figs. 8b, 8d, 8e and 8f. These were obtained on the same model at a station further aft, at 66 per cent of the model length, in the 8 ft × 8 ft tunnel at R.A.E. Bedford. The upper-surface distribution shown in Fig. 8b looks entirely consistent with the trend of the present results; the lower-surface pressure show a slightly different trend near the leading edge. The position of the maximum suction is remarkably constant over the range $0{\cdot}9 \leqslant M \leqslant 2$ for which the secondary separation is laminar.

At $\alpha = 12°$, Fig. 8c, there is an indication that the lifting pressure on the lower surface and the suction on the inboard part of the upper surface both increase with M up to 0·9 or 1·0 and then fall off. This is the trend that linear theory would predict. The two suction peaks of turbulent type at $M = 0{\cdot}4$ and 0·6 are more nearly the same. As at the higher incidences, there is a marked drop in peak suction between

$M = 0{\cdot}6$ and $0{\cdot}82$, at which Mach number the suction peak takes an intermediate form. The peaks at $M = 1{\cdot}0$ and $1{\cdot}1$ probably correspond to conical flow with a laminar secondary separation. The main shift in the position of the maximum suction is again associated with the change in the shape of the peak.

At $\alpha = 8°$, Fig. 8d, there is again an indication that the pressure on the lower surface and the suction on the inboard part of the upper surface reach maximum values near $M = 0{\cdot}9$ to $1{\cdot}0$. The suction peaks are now all of the type associated with turbulent separation. There is a marked reduction in peak suction from $M = 0{\cdot}4$ to $M = 2{\cdot}0$, proceeding steadily through the results taken from Britton[5], but the reduction is halted and possibly reversed between $M = 0{\cdot}82$ and $1{\cdot}0$. The inboard movement of the peak is less than 3 per cent of the semi-span.

At $\alpha = 6°$ and $4°$, Figs. 8e and 8f, the variations in lifting pressure are so small that attention has been concentrated on the suction peak and many curves for intermediate Mach numbers have been omitted. At $6°$ the suction peaks are of the turbulent type, except perhaps at $M = 2$. At $\alpha = 4°$ the secondary separation is probably laminar at all Mach numbers. At both incidences the consistency of the results over a substantial range of subsonic and supersonic Mach numbers is remarkable.

The descriptions of the suction peaks can now be summarised conveniently in Table 1. We use letters *T*, *L* and *I* to denote suction peaks corresponding to secondary separations which are turbulent or laminar or peaks of an intermediate shape.

TABLE 1

Summary of Suction-Peak Shape, Re $= 2 \times 10^6$

M \ α	4°	6°	8°	12°	16°	20°
0·4	*L*	*T*	*T*	*T*	*T*	*T*
0·6	*L*	*T*	*T*	*T*	*T*	*T*
0·82	*L*	*T*	*T*	*I*	*I*	*I*
0·9	*L*	*T*	*T*	*I*	*L*	*I*
1·0	*L*	*T*	*T*	*L*	*L*	*L*
1·1	*L*	*T*	*T*	*L*	*L*	*L*

Comparison of Figs. 8a to 8e shows that the overall variation of peak suction for given incidence between $M = 0{\cdot}4$ and $1{\cdot}1$ decreases as the incidence decreases, both absolutely and in relation to the value of the peak suction. This is brought out in Fig. 9, which presents the peak lifting suctions from Fig. 8 as functions of Mach number. Points for intermediate Mach numbers are given where these were measured and some additional values are taken from Britton[5]. Against each point a letter *T*, *L* or *I* appears, on the basis of Table 1. This is certainly helpful in explaining the variation at $\alpha = 12°$, the point at $M = 1{\cdot}3$ being obtained from Britton's measurements at a Reynolds number of 8 million.

At the lowest incidence (4°) the variation in peak lifting suction is small and there is no significant variation through the transonic range, $0{\cdot}82 \leqslant M \leqslant 1{\cdot}1$. This is what would be expected from slender-body theory, as described in Appendix A. At higher incidences, the peak lifting suction falls as Mach number increases, and the fall is steeper the higher the incidence. The fall is not only in the transonic range, where Heaslet and Spreiter[15] have warned us that slender-body theory is limited to incidences of the size of the thickness ratio, but also between $M = 0{\cdot}4$ and $0{\cdot}6$. At $\alpha = 8°$, where there is already a

significant fall, the local Mach number at the peak is just above 0·7 for $M = 0{\cdot}6$, but it has risen to 0·91 for $\alpha = 20°$ at $M = 0{\cdot}6$. As an indication of where compressibility effects can be expected to be large, the 'critical lifting pressure coefficient' is shown in Fig. 9. This is defined by

$$C_{p_L}|_{\text{critical}} = C_p|_{\text{critical}} - C_p|_{\alpha=0} \tag{1}$$

where

$$C_p|_{\text{critical}} = \frac{2}{\gamma M^2}\left[\left\{1-\frac{\gamma-1}{\gamma+1}(1-M^2)\right\}^{\frac{\gamma}{\gamma-1}}-1\right], \quad \text{as usual,} \tag{2}$$

and

$$C_p|_{\alpha=0} = 0{\cdot}024+0{\cdot}117\,M\,. \tag{3}$$

The last relation roughly represents the variation with Mach number of the pressure coefficient at zero incidence over that part of the wing surface where the suction peak occured in the present tests.

The other curves shown on Fig. 9 are straight lines drawn through the measured peak suction for $M = 1$ with the slopes

$$\frac{dC_{p_L}}{dM} = -\frac{2}{\gamma+1}C_{p_L}|_{M=1} \text{ for } \gamma = 1{\cdot}4\,. \tag{4}$$

This is the variation of lifting pressure coefficient with free-stream Mach number which would make the rate of change of local Mach number with free-stream Mach number vanish for a sonic free-stream, in other words, the variation of lifting pressure coefficient corresponding to the 'Mach number freeze'. Although wrong in detail, the predictions of this semi-empirical rule are surprisingly close.

The substantial reductions in the peak suction shown in Fig. 9 as M increases from 0·4 to 1·0 are not in conflict with the observations of Squire and Capps[2] and Squire[3] that both the linear and non-linear parts of the lift on slender wings at given incidence increase as the Mach number rises towards one. Two effects evident in the present results counteract the reduction in peak suction. In Fig. 8 an increase in lower-surface pressure with Mach number can be seen, particularly at the higher incidences, and Fig. 6 shows how, at the higher Mach numbers, the suction is carried closer to the trailing edge.

In any consideration of conical compressible flow, it is important to know whether the flow is conically supersonic anywhere, since it is only in regions of conically supersonic flow that conical shock waves can occur. The appropriate condition is that the component of the velocity normal to a ray through the apex should be supersonic. Since, in the present experiments, the flow was not strictly conical, measurements were confined to the wing and only the static pressure was measured, no more than a tentative answer can be given. Fortunately, what evidence there is suggests that in flows with leading-edge vortices the velocity component normal to the ray is largest just outside the boundary layer on the wing. For instance, Fig. 20 of Ref. 4 shows cross-flow velocities calculated for a flat-plate delta wing at an incidence just less than one-half of its apex angle. There, although the addition of the free-stream component of $U(y^2+z^2)^{1/2}/x$ directed towards the origin increases the normal component above the vortex and decreases it below, the maximum still seems to lie on the wing surface. Fig. 10 of Ref. 17 shows cross-flow velocities measured at low speed on a thin wing at an incidence equal to one-half the apex angle. Again the maximum velocity normal to the rays occurs near the wing surface. The measurements reported in Ref. 8 on a thicker wing in a supersonic flow are not at close enough intervals to provide information on the maximum of the normal velocity, but they suggest it is still roughly the same above and below the vortex. Hence, we suppose that if the flow is not conically supersonic at the edge of the wing boundary layer, then it is not conically supersonic elsewhere (except ahead of the bow shock when $M_\infty > 1$).

It is shown in Appendix C that the separate velocity components can be derived from the measured static pressure provided the flow is attached. For conical flow with lateral symmetry the problem reduces to the integration of an ordinary differential equation outwards from the plane of symmetry and the method is valid inboard of the secondary separation line. Since secondary separation occurs somewhat

outboard of the suction peak and velocity maximum, this approach is adequate to determine whether the flow on the wing is conically supersonic.

Since the measured pressure distributions are less conical than the lifting pressure distributions, in terms of which the results have been discussed so far, it is arguable that the lifting pressure distribution forms a more appropriate basis for calculating the flow direction on the wing. Fortunately it is not necessary to resolve this point. Since the zero-lift pressure coefficient is positive, the lifting pressure is lower than the measured and the corresponding velocities are higher. Using the lifting pressure distribution to perform the calculation described in Appendix C, we find that the maximum Mach number normal to a ray is always less than one for the present tests. Since it would be lower still if the measured pressures were used, we can conclude that, as far as the concept is meaningful for flows only approximately conical, the flow fields in the present experiments were nowhere conically supersonic (except ahead of the bow shock for $M_\infty > 1$).

The largest Mach numbers normal to the rays naturally occurred at the largest incidence. For the upper-surface distributions of lifting pressure shown in Fig. 8a for $\alpha = 20°$ we found:

Free-stream Mach number	0·4	0·6	0·82	0·9	1·0	1·1
Max. Mach number normal to ray	0·41	0·58	0·75	0·83	0·89	0·94

For the lifting pressure distribution derived from Britton's results[5] at $\alpha = 16°$, $M = 2$ (Fig. 8b), the Mach number normal to the ray was as high as 2·8. For the measured pressure distribution the corresponding value was only 1·4, but it is clear that conically supersonic conditions do occur at higher Mach numbers. It is also possible that conically supersonic conditions might have occurred in the present tests if the secondary separation at $M = 1·1$, $\alpha = 20°$ had been turbulent instead of laminar (cf. Fig. 7b for the marked effect of transition on peak suction).

4. *Conclusions.*

(a) The investigation of the effect of Mach number on the lifting pressure on a slender sharp-edged conical body was complicated by an unexpected change in the Reynolds number based on the station at which transition occurred in the secondary boundary layer under the leading-edge vortex. At the lower Mach numbers, the results were consistent with previous low-speed observations, in that the secondary separation was turbulent for incidences above 4°. At higher subsonic and transonic Mach numbers laminar secondary separations were found at incidences above 8°.

(b) In spite of this effect, which produced changes in the shape of the suction peaks at the principal lengthwise measuring station, it was possible to show a steady reduction in the magnitude of the peak suction as the Mach number increased, both in the separate families which correspond to laminar and turbulent separation and also overall. It has not been possible to explain the variation in the peak suction with Mach number. However, the variation appears to be continuous and no regions of conically supersonic flow, in which conical shocks would be possible, are found. The flow is therefore of the same type as that postulated in treatments of the vortex sheet model of leading-edge separation by slender-body theory, such as Ref. 4.

(c) The reduction in peak suction measured at the principal measuring station, which lay forward, where the lifting pressure field was almost conical, was counteracted in its effect on lift by two other features. As the Mach number increased subsonically, the lifting pressure field was maintained in its almost conical form further back towards the trailing edge. Also, increases in pressure on the lower surface and suction on the inboard part of the upper surface were found.

(d) The lateral position of the peak suction, which has previously been found to correlate with the lateral position of the vortex, moves slightly inboard as Mach number increases, but most of this movement is associated with the change from turbulent to laminar secondary separation.

(e) Since it is the lateral position of the vortex which is most in error in the calculations by Smith[4] for flat-plate wings, and the calculated positions are further outboard than the low-speed observations on thin wings, it is unlikely that better agreement with these slender-body theory calculations will be found at transonic speeds than at low speeds.

LIST OF SYMBOLS

A	Aspect ratio
b	Tunnel breadth
b_0	*See* Appendix A
B	Base area of model
c	Wing length
C_L	Lift coefficient
C_p	Pressure coefficient
C_{pL}	Lifting pressure coefficient ($= C_p - C_p\|_{\alpha=0}$)
g	Parameter depending on slot configuration
I	Indicates an intermediate form of suction peak
l	Body length
L	Indicates a 'laminar' suction peak
M	Mach number
R	Radius of tunnel section
Re	Reynolds number
s	Local semi-span of wing
S	Local cross-sectional area of body
T	Indicates a 'turbulent' suction peak
U	Free-stream speed
x, y, z	Right-handed Cartesian axes, origin at wing apex, Ox downstream, Oy to starboard
α	Incidence
γ	Adiabatic index
ε	*See* Appendix B
λ	Height to breadth ratio of tunnel
τ	Thickness ratio of model
ϕ	Velocity potential

REFERENCES

No.	*Author(s)*	*Title, etc.*
1	D. Küchemann	On some three-dimensional flow phenomena of the transonic type. *Proc. I.U.T.A.M. Symposium Transsonicum*, Aachen p 218, Springer, Berlin (1964).
2	L. C. Squire and D. S. Capps..	An experimental investigation of the characteristics of an ogee wing from $M = 0{\cdot}4$ to $M = 1{\cdot}8$. A.R.C. C.P. 585 (1959).
3	L. C. Squire	The characteristics of some slender cambered gothic wings at Mach numbers from 0·4 to 2·0. A.R.C. R. & M. 3370 (1962).
4	J. H. B. Smith	Improved calculations of leading edge separation from slender delta wings. R.A.E. Technical Report 66070 (A.R.C. 27897) (1966).
5	J. W. Britton	Pressure measurements at supersonic speeds on three uncambered conical wings of unit aspect ratio. A.R.C. C.P. 641 (1962).
6	D. Hummel	Experimentelle Untersuchung der Strömung auf der Saugseite eines schlanken Deltaflügels. *Zeitschrift für Flugwissenschaften*, **13**, pp 247–252 (1965).
7	N. Gregory and E. M. Love ..	Some problems of flow laminarization on a slender delta wing. N.P.L. Aero Report 1138, (A.R.C. 26754) (1965).
8	L. Gaudet and K. G. Winter ..	Preliminary measurements of the flow field on the leeside of a delta wing of unit aspect ratio at a Mach number of 2·6 and an incidence of 15°. R.A.E. Technical Note Aero 2787 (A.R.C. 23510) (1961).
9	S. B. Berndt	Wind tunnel interference due to lift for delta wings of small aspect ratio. K.T.H. (Sweden) Aero Technical Note 19 (1950).
10	P. B. Earnshaw and J. A. Lawford	Low-speed wind-tunnel experiments on a series of sharp-edged delta wings. Part 1—Forces, moments, normal force fluctuations and positions of vortex breakdown. A.R.C. R. & M. 3424 (1961).
11	D. L. I. Kirkpatrick	Investigation of the normal force characteristics of slender delta wings with various rhombic cross-sections in subsonic conical flow. A.R.C. C.P. 922 (1965).
12	S. B. Berndt	Theoretical aspects of the calibration of transonic test sections. F.F.A. (Sweden) Report 74 (1956).

REFERENCES—*continued*

No.	*Author(s)*	*Title, etc.*
13	J. A. Lawford	Low-speed wind-tunnel experiments on a series of sharp-edged delta wings. Part 2—Surface flow patterns and boundary-layer transition measurements. A.R.C. R. & M. 3424 (1964).
14	D. A. Lemaire	Some observations of the low-speed flow over a sharp-edged delta wing of unit aspect ratio. A.R.L. (Australia) Aero Report 126 (1965).
15	M. A. Heaslet and J. R. Spreiter	Three-dimensional transonic flow theory applied to slender wings and bodies. NACA Technical Note 3717 (1956).
16	G. N. Ward	*Lineraised theory of steady high-speed flow.* Cambridge University Press (1955).
17	S. C. Russell	The effects of conical thickness on the flow about low aspect ratio wings with sharp leading edges. University of Salford, Mechanical Engineering Department, Project Report (1966).

APPENDIX A

The 'Lifting Pressure Field' for a Symmetrical Slender Body.

In the analysis of pressure measurements on symmetrical thin wings at small incidences, when the pressure is expected to be linearly related to the inclination of the surface of the wing to the flow, it is usual to subtract the pressure measured at zero incidence from the results, to obtain a pressure distribution due to lift. In the present tests no such linear relation could be expected; but there is a possibility that the pressure distribution may be calculable by slender-body theory, with some representation of the leading-edge vortices. In this theory, the boundary condition is applied on the actual body surface; the first approximation to the pressure coefficient involves the square of the cross-flow velocity; and, at transonic speeds, the governing differential equation is non-linear. It would be dangerous therefore to carry over ideas based on fully linearised theories to the present measurements; but this Appendix shows that, according to slender-body theory, the 'lifting pressure field' obtained by subtracting the pressures at zero incidence is independent of Mach number and, for a conical body is conical. At transonic speeds, the independence of Mach number is restricted to small incidences, typically less than the thickness-to-chord ratio of the body. (Heaslet and Spreiter[15].)

With a system of right-handed axes $Oxyz$, in which O is the apex of the body and Ox is parallel to the undisturbed stream, the velocity potential, ϕ, in the slender-body approximation for subsonic and supersonic speeds can be written (*see* Ward[16] pp 194–200) as:

$$\phi = U(x+\phi_0), \tag{5}$$

where

$$\phi_0 = \frac{1}{2\pi} S'(x) \log r + b_0(x) + \phi_1 . \tag{6}$$

Here $S(x)$ is the cross-sectional area of the body; $r^2 = y^2+z^2$; ϕ_1 is a solution of Laplace's equation in the cross-flow plane

$$\frac{\partial^2 \phi_1}{\partial y^2} + \frac{\partial^2 \phi_1}{\partial z^2} = 0 , \tag{7}$$

such that $\nabla\phi_1 \to 0$ as $r \to \infty$; and $b_0(x)$ is a function which takes different forms for subsonic and supersonic speeds. For subsonic flow, with $\beta^2 = 1-M^2$,

$$2\pi\, b_0(x) = S'(x) \log(\beta/2) + 1/2 \int_x^1 S''(t) \log(t-x)\, dt$$

$$- 1/2 \int_0^x S''(t) \log(x-t)\, dt . \tag{8}$$

For supersonic flow, with $B^2 = M^2-1$,

$$2\pi\, b_0(x) = S'(x) \log (B/2) - \int_0^x S''(t) \log(x-t)\, dt . \tag{9}$$

For transonic flow a similar expression can be given for ϕ_0, provided the incidence is small, typically less than the thickness ratio of the body, as shown by Heaslet and Spreiter[15]. No explicit representation of $b_0(x)$ is possible, though.

For a slender body, $\partial\phi_0/\partial x << 1$ almost everywhere on the body. Consequently, the boundary condition that the velocity component normal to the body surface vanishes becomes a condition which relates the component of velocity lying in the cross-flow plane and normal to the body cross-section to the body shape, the incidence and the free-stream velocity. The body boundary condition does not, therefore, involve $b_0(x)$. If the flow field contains a vortex sheet, an additional boundary condition must be satisfied on it, namely that the pressure is continuous across it. This condition can also be formulated in terms of differences in ϕ at the same value of x and derivatives of ϕ in the cross-flow plane. Hence ϕ_1 is independent of $b_0(x)$ and so, in particular, independent of Mach number.

For a conical body with conical vortex sheets, the boundary conditions will be satisfied by velocities in the cross-flow plane which are constant along rays through the apex. Such velocities derive from a potential which is a homogeneous function of the first order and since $S'(x)$ is proportional to x, ϕ_1 will be such a homogeneous function.

The pressure coefficient is given, in the slender-body approximation, by

$$C_p = -2\frac{\partial\phi_0}{\partial x} - \left(\frac{\partial\phi_0}{\partial y}\right)^2 - \left(\frac{\partial\phi_0}{\partial z}\right)^2 \tag{10}$$

In this, effects of Mach number enter only through $\partial\phi/\partial x$, since ϕ_1 has been shown to be independent of Mach number. But this term in C_p is linear, and the term in ϕ depending on Mach number is independent of incidence, so the dependence on Mach number disappears when C_p at zero incidence is subtracted to give the 'lifting pressure field'. Moreover, for a conical slender body, $\partial\phi_0/\partial x$ is the only term in C_p which is not constant on conical rays, and the only term in $\partial\phi_0/\partial x$ which is not constant on conical rays is $b_0'(x)$. Hence for a conical body the 'lifting pressure field' is conical.

APPENDIX B

Blockage Correction for Solid Walls at Low Speeds.

The method used by Kirkpatrick[11] supposes that the displacement effect of the model and its wake can be represented by a linear source distribution along the centreline of the tunnel, with a point sink of the same total strength at infinity downstream. The strength of the source distribution is proportional to the rate of change of cross-sectional area of the model and the wall boundary conditions are satisfied by introducing a doubly-infinite array of images.

He expresses the blockage correction ε in the form

$$\Delta U/U = \varepsilon = \varepsilon_2 + \varepsilon_1 (x/c) : \tag{11}$$

where ε_1 is the contribution from the linear source distribution and depends on the streamwise station, x/c, and ε_2 is the contribution from the sink at infinity. He finds

$$\varepsilon_1 = \frac{B}{2\pi c^2} \sum_{m,n=-\infty}^{\infty}{}' k_1 \left(\frac{x}{c}, \frac{b}{c} \sqrt{m^2 \lambda^2 + n^2} \right) \tag{12}$$

and

$$\varepsilon^2 = B/2\lambda b^2 \tag{13}$$

where

$$k_1 \left(\frac{x}{c}, \frac{y}{c} \right) = \frac{c}{\sqrt{(x-c)^2 + y^2}} - \log \frac{x + \sqrt{x^2 + y^2}}{x - c + \sqrt{(x-c)^2 + y^2}}, \tag{14}$$

$\sum'$ denotes the double sum excluding $m = n = 0$, c = model length, B = model base area, b = tunnel breadth, λ = tunnel height to breadth ratio and each pair of integers (m, n) refers to one of the doubly-infinite set of images of the tunnel centreline in the tunnel walls.

For the present purpose the double sum has been evaluated in the form

$$\sum_{m,n=-\infty}^{\infty}{}' f(m, n) = \lim_{r \to \infty} \sum_{s=1}^{r} F(s), \tag{15}$$

where

$$F(s) = 2f(0, s) + 2f(s, 0) + 4f(s, s) + 4 \sum_{m=1}^{s-1} (f(m, s) + f(s, m)); \tag{16}$$

that is to say, all the images lying on a rectangle similar in shape to the tunnel section are taken together and the final sum is over all such rectangles. The convergence as $r \to \infty$ is not very fast. We find

$$k_1\left(\frac{x}{c}, \frac{y}{c}\right) \sim A_1\left(\frac{c}{y}\right)^3 \quad \text{for } y/c \text{ large},$$

and so,

$$F(s) \sim A_2\left(\frac{1}{s}\right)^2 \quad \text{for } s \text{ large}. \tag{17}$$

This suggests how the convergence can be accelerated. We write

$$\sum_{s=1}^{\infty} F(s) = \sum_{s=1}^{r} F(s) + \sum_{s=r+1}^{\infty} \frac{a(s)}{s^2},$$

where $a(s)$ is nearly constant for $s > r$, if r is large enough.
Therefore,

$$\sum_{s=r+1}^{\infty} \frac{a(s)}{s^2} \simeq a(r) \sum_{s=r+1}^{\infty} \frac{1}{s^2} = r^2 F(r)\left(\frac{\pi^2}{6} - \sum_{s=1}^{r} \frac{1}{s^2}\right)$$

therefore,

$$\sum_{s=1}^{\infty} F(s) = \lim_{r \to \infty}\left\{\sum_{s=1}^{r} \left(F(s) - \frac{r^2 F(r)}{s^2}\right) + \frac{\pi^2}{6} r^2 F(r)\right\}. \tag{18}$$

The convergence of the term in braces is now rapid. In Kirkpatrick's case, for $x = 0, F(10) = -0{\cdot}0124$, but the difference between the term in braces for $r = 9$ and $r = 10$ is only $-0{\cdot}0002$.

In the present case, $c = 2{\cdot}75$ feet, $B = 0{\cdot}546$ square feet, $b = 8$ feet and $\lambda = 0{\cdot}75$, so that $\varepsilon_2 = 0{\cdot}0057$. At the forward station $x/c = 0{\cdot}336$, $\Sigma' = -0{\cdot}087$, $\varepsilon_1 = -0{\cdot}0010$ and so $\varepsilon = 0{\cdot}0047$. At the aft station, $x/c = 0{\cdot}601$, $\Sigma' = -0{\cdot}019$, $\varepsilon_1 = -0{\cdot}0002$ and so $\varepsilon = 0{\cdot}0055$.

APPENDIX C

Calculation of Velocity Components from Pressure Coefficient.

From the values of the pressure coefficient, C_p, obtained from the measured pressures, Bernoulli's equation expresses the speed, v, of the flow external to the boundary layer in terms of the free-stream Mach number, M_∞, and the free-stream speed, v_∞:

$$\left(\frac{v}{v_\infty}\right)^2 = 1-\frac{2}{(\gamma-1)M_\infty^2}\left[\left(1+\frac{\gamma M_\infty^2 C_p}{2}\right)^{\frac{\gamma-1}{\gamma}}-1\right] \tag{19}$$

The velocity, $\mathbf{v}$, at a point at the edge of the body boundary layer is tangential to the body surface (or, more precisely, the displacement surface), so

$$\mathbf{v}\,.\,\mathbf{n} = 0\,, \tag{20}$$

where $\mathbf{n}$ is a vector normal to the body surface. Provided the flow is attached, no vortex line enters the external flow from the boundary layer and so

$$\boldsymbol{\omega}\,.\,\mathbf{n} = 0\,, \tag{21}$$

where $\boldsymbol{\omega} = \nabla\wedge\mathbf{v}$ is the vorticity vector. If (21) is supplemented by boundary values on an appropriate initial line, the three equations (19), (20) and (21) determine the velocity components in some neighbourhood of the initial line in which the flow remains attached.

We are concerned with conical, laterally symmetric flow over plane surfaces only, so it is convenient to choose a set of rectangular axes with O at the apex, Oz along the outward normal to the surface, Ox in the plane of symmetry and Oy completing the right-handed system. Then, if

$$\mathbf{v} = \mathbf{i}\,v_x+\mathbf{j}\,v_y+\mathbf{k}\,v_z\,,$$

equation (20) becomes simply

$$v_z = 0$$

and (21) becomes

$$\frac{\partial v_x}{\partial y} = \frac{\partial v_y}{\partial x}\,. \tag{22}$$

For conical flow, v_x and v_y depend solely on the polar angle θ, where $x = r\cos\theta$ and $y = r\sin\theta$. Hence (22) becomes

$$\frac{dv_x}{d\theta}\cos\theta+\frac{dv_y}{d\theta}\sin\theta = 0\,, \tag{23}$$

since $\dfrac{\partial\theta}{\partial y} = \dfrac{\cos\theta}{r}$ and $\dfrac{\partial\theta}{\partial x} = -\dfrac{\sin\theta}{r}$. We now introduce v_r and v_θ, the components of $\mathbf{v}$ in the directions of increasing r and θ respectively. Then

$$v_r = v_x\cos\theta+v_y\sin\theta$$

and

$$\frac{dv_r}{d\theta} = \frac{dv_x}{d\theta}\cos\theta + \frac{dv_y}{d\theta}\sin\theta - v_x\sin\theta + v_y\cos\theta$$

$$= (\text{by (23)})\, v_\theta . \tag{24}$$

On the surface, $v_r^2 + v_\theta^2 = v^2$ and so, introducing

$$f(\theta) = \frac{v}{v_\infty}$$

and

$$g(\theta) = \frac{v_r}{v_\infty}$$

we have

$$g^2 + g'^2 = f^2 \tag{25}$$

where f is known from (19). This is an ordinary differential equation of the first order and the second degree, for which a single boundary condition is required. In the present case we have $v_\theta = 0$ for $\theta = 0$ by symmetry, and so

$$g'(0) = 0 . \tag{26}$$

A pair of analytic solutions of (25) exists only for very special choices of the function f. For the case $f = f_0$, a constant, there are two solutions satisfying (26), *viz*

$$g = f_0 \quad \text{and} \quad g = f_0 \cos\theta . \tag{27}$$

These correspond to a radial outflow from the apex and a parallel flow. The equation can be reduced to a pair of equations of Abel type by the successive substitutions $g = f\cos u$ and $h = \tan u$. The result is

$$fhh' - (1+h^2)f' \pm (1+h^2)fh = 0 . \tag{28}$$

Equation (25) has a simple geometrical interpretation. If g represents the radial distance of a point from the origin of polar co-ordinates and θ is the polar angle, f represents the derivative of the arc length with respect to θ. Solving the equation corresponds to finding the curves whose arc lengths are a given function of the polar angle. The two solutions (27) obviously correspond to a pair of circles of radii f_0 and $f_0/2$ which touch internally at $\theta = 0$.

The numerical integration of (25) presents difficulties in general since solution curves branch at points where $g' = 0$ and it is not easy to follow both branches. In particular, starting from (26) with $f = f_0$, most methods of integration only give the solution $g = f_0$. This is not the solution most likely to be appropriate in the present case, where a region of constant pressure near the plane of symmetry probably corresponds to a region of parallel flow. A further difficulty arises when f initially decreases as θ increases, i.e. $f''(0) < 0$. No real solution exists if f decreases rapidly: if f decreases gradually and a solution does exist, special procedures are needed to deal with the negative values found for g'^2 in the Runge-Kutta process. The use of (28) would avoid some of these difficulties, but would require values of f' as data. Deriving these from measurements of f would introduce uncertainties.

Fortunately, it is sufficient for the purpose of the present Report to consider only the case where the pressure begins to fall quite close to the plane of symmetry and continues to fall monotonically to its overall minimum, as illustrated by Fig. 8a. This means that we can take $f(\Delta) > f(0)$ in all cases, where Δ is either the integration interval or the first data point away from the plane of symmetry. There is then no difficulty in obtaining a pair of solutions which extend beyond the value of θ at which the occurrence of secondary separation invalidates equation (21). It is not obvious *a priori* whether the physically realistic solution will arise from the positive or negative value of g', so both solutions have been programmed for numerical solution by the Runge-Kutta method. In the cases computed only one of the solutions produced $v_y > 0$ near the suction peak and this was clearly the one appropriate to the real flow.

TABLE 2

Positions of Static Pressure Holes.

Along the semi-span		Along the generator
at $\frac{x}{c} = 0{\cdot}336$	at $\frac{x}{c} = 0{\cdot}601$	at $\frac{y}{s} = 0{\cdot}597$
$\frac{y}{s}$	$\frac{y}{s}$	$\frac{x}{c}$
0·014	0·102	0·050
0·040	0·202	0·100
0·069	0·300	0·150
0·096	0·353	0·200
0·125	0·399	0·250
0·150	0·450	0·300
0·200	0·500	0·350
0·249	0·547	0·400
0·300	0·599	0·450
0·353	0·647	0·500
0·400	0·697	0·550
0·450	0·750	0·600
0·500	0·801	0·700
0·550	0·848	0·800
0·601	0·875	0·902
0·660	0·897	
0·703	0·924	
0·750	0·952	
0·801		
0·851		
0·875		
0·900		
0·926		
0·951		
0·971		

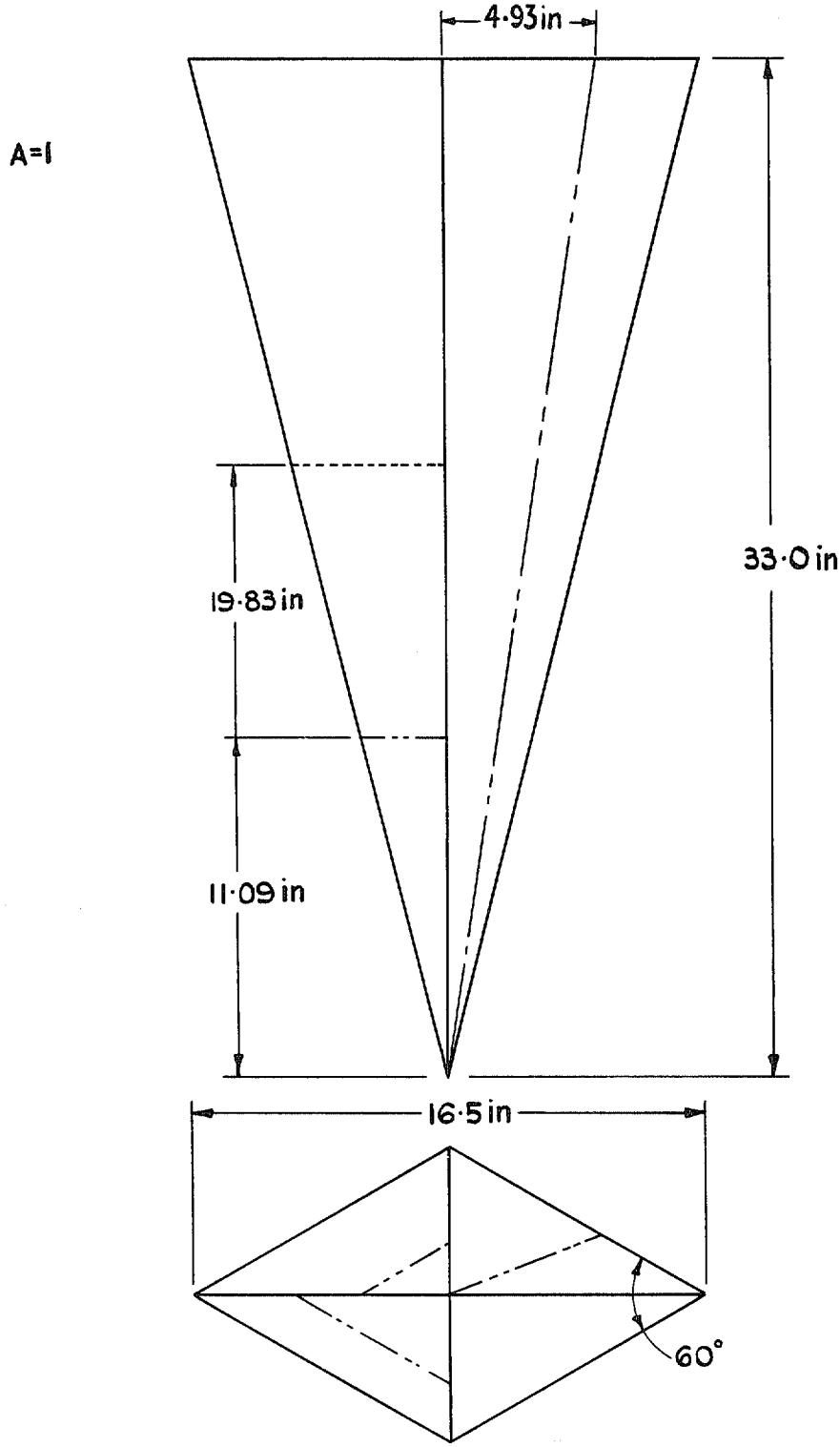

FIG. 1. Model dimensions and pressure measuring stations.

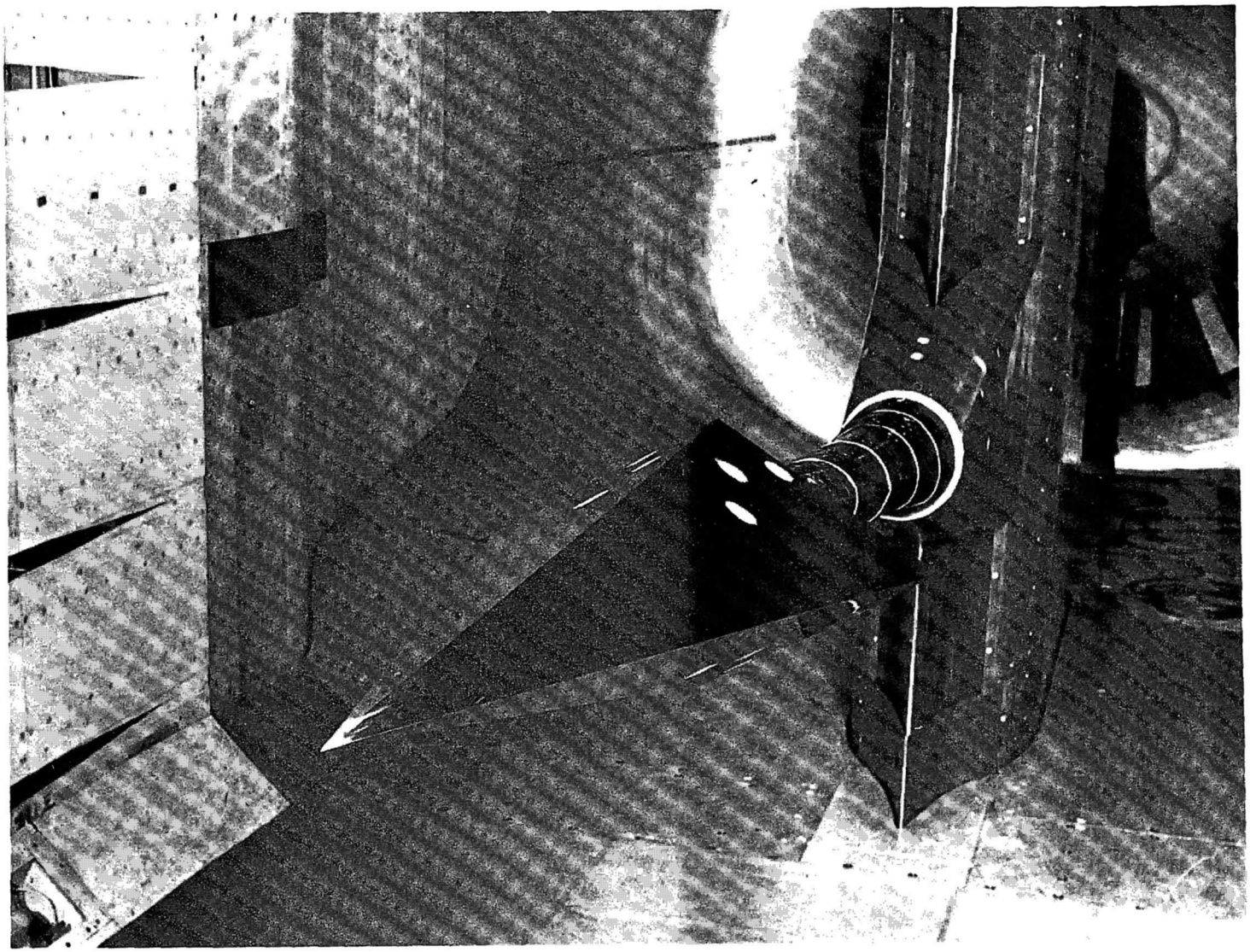

FIG. 2. Model mounted in working section of tunnel.

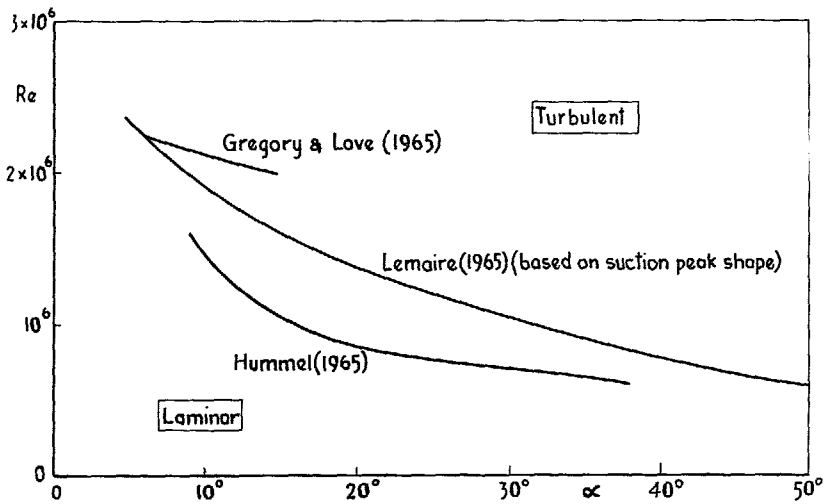

FIG. 3. Reynolds number based on distance from apex of transition in secondary boundary layer at low speeds on delta wings of aspect ratio one (based on Refs. 6, 7 and 14).

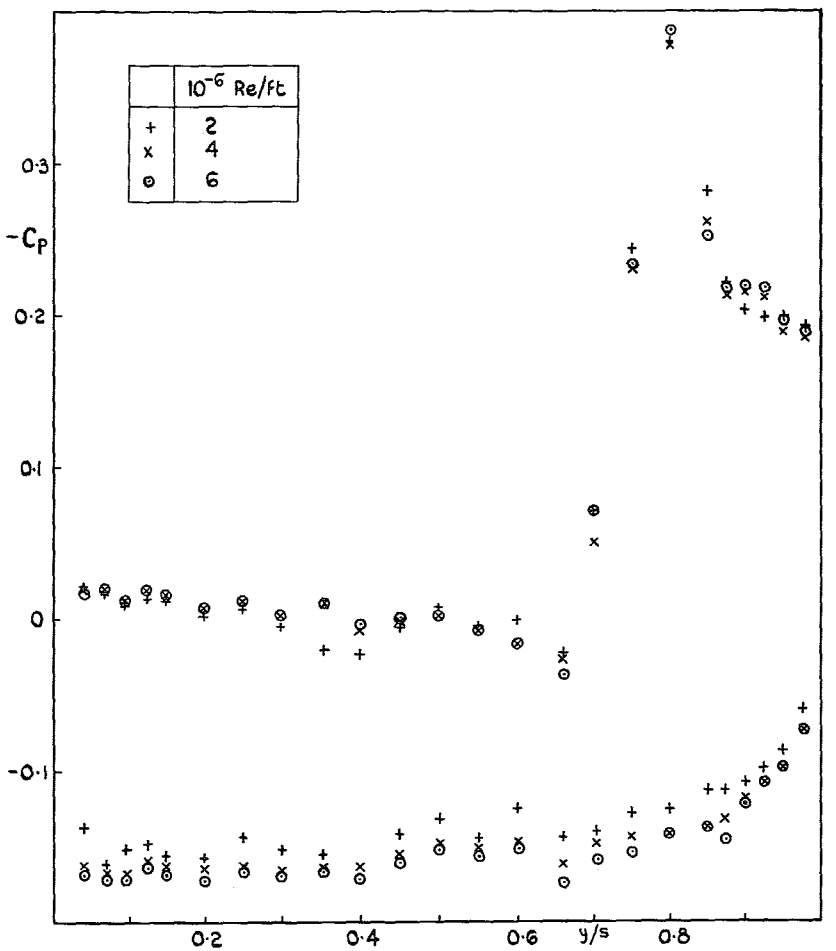

FIG. 4a. Pressure distribution at forward station, transition free. $M = 0{\cdot}4$, $\alpha = 8°$, various Reynolds numbers.

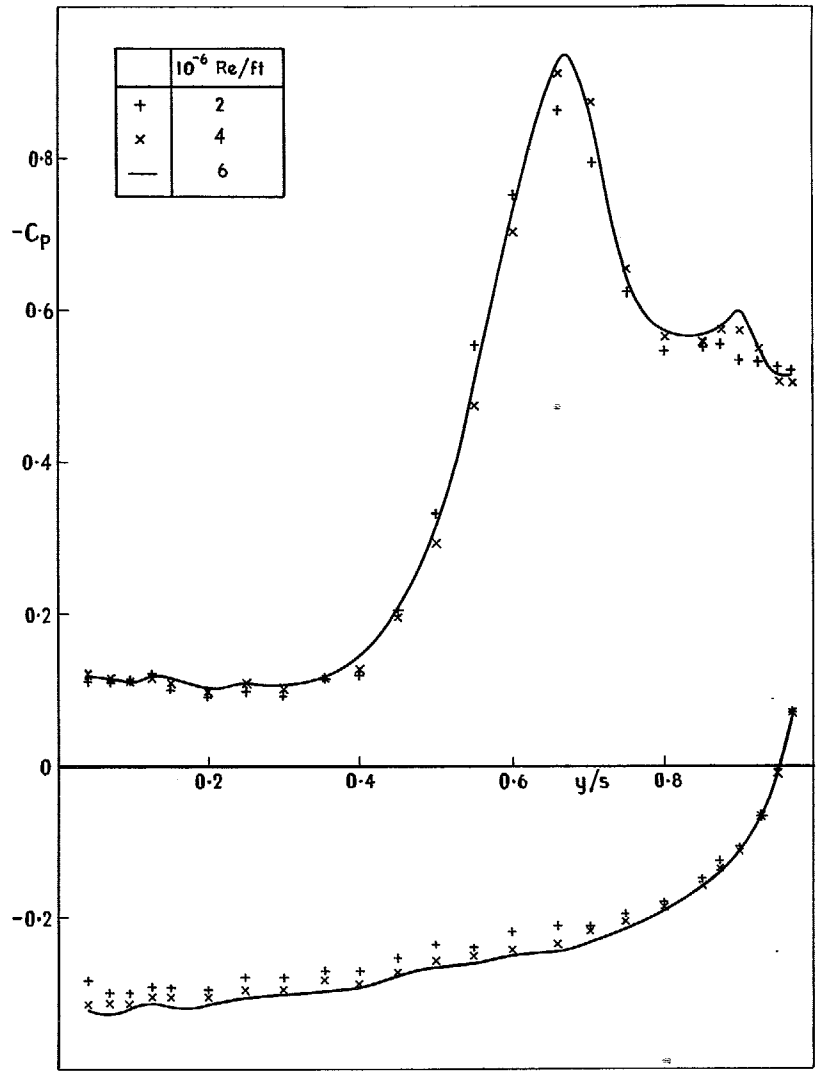

FIG. 4b. Pressure distribution at forward station, transition free, $M = 0{\cdot}4$, $\alpha = 16°$, various Reynolds numbers.

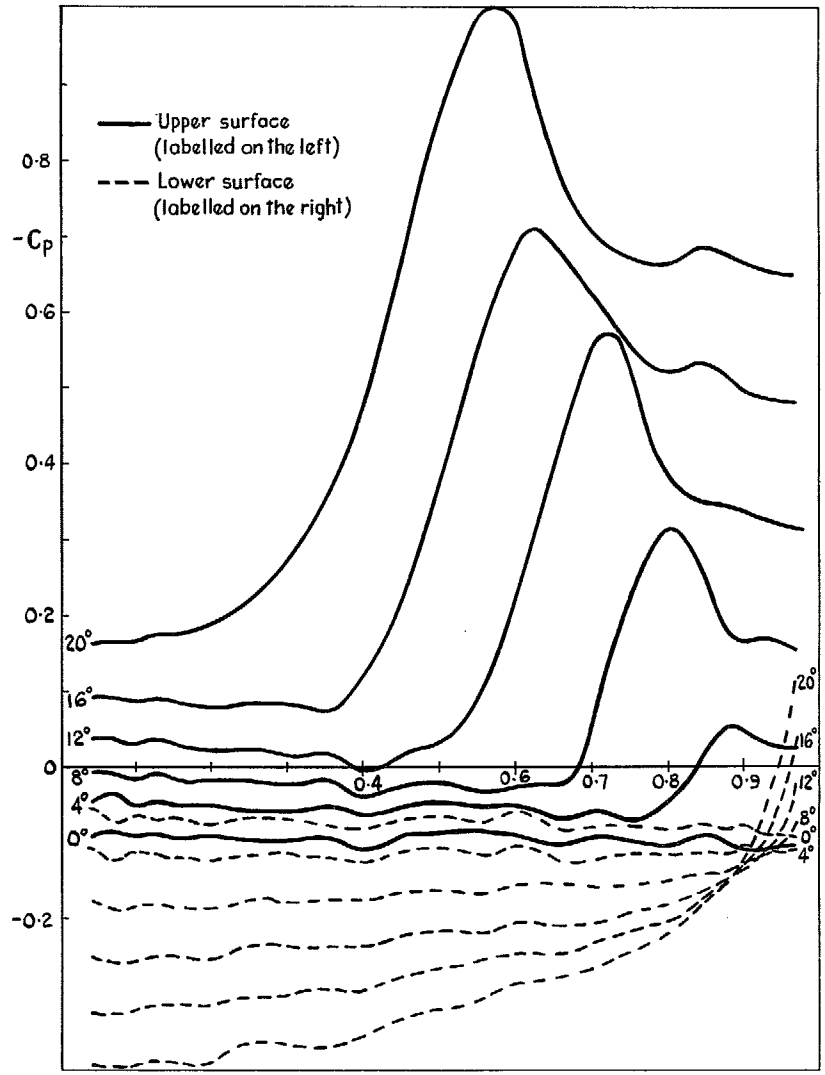

FIG. 5a. Pressure distributions at forward station, transition free, $M = 0{\cdot}6$, various incidences.

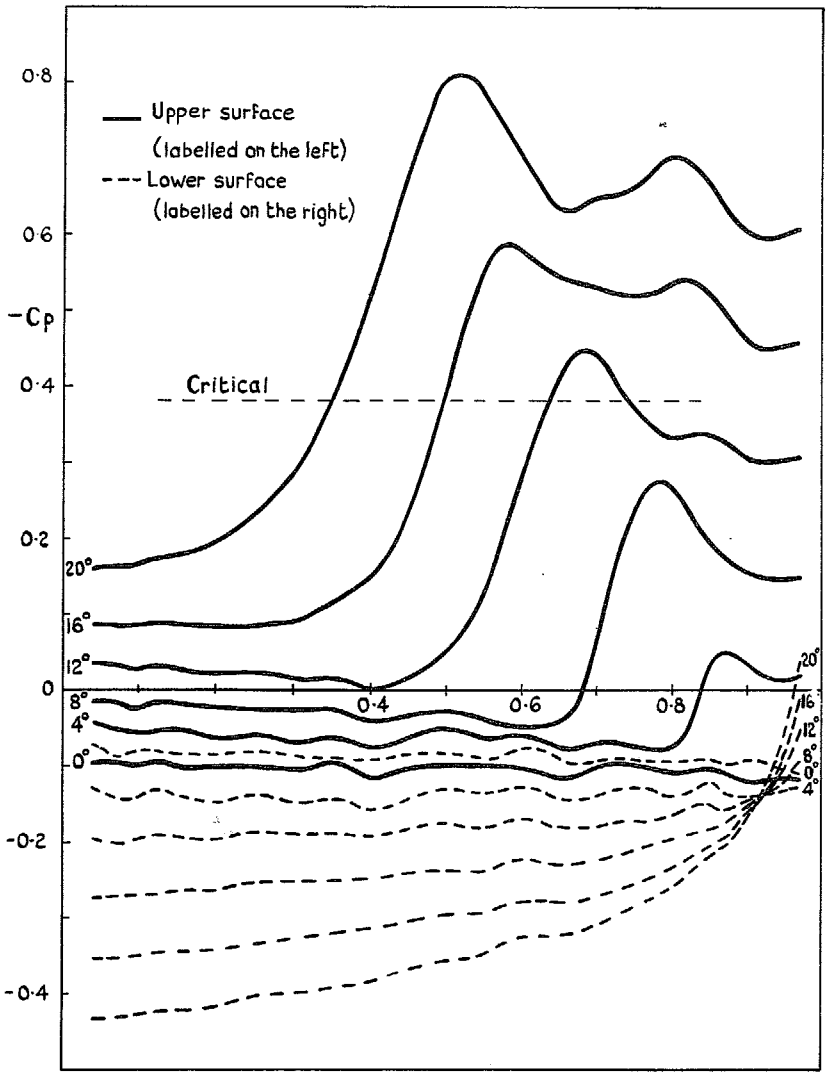

FIG. 5b. Pressure distributions at forward station, transition free. $M = 0{\cdot}82$, various incidences.

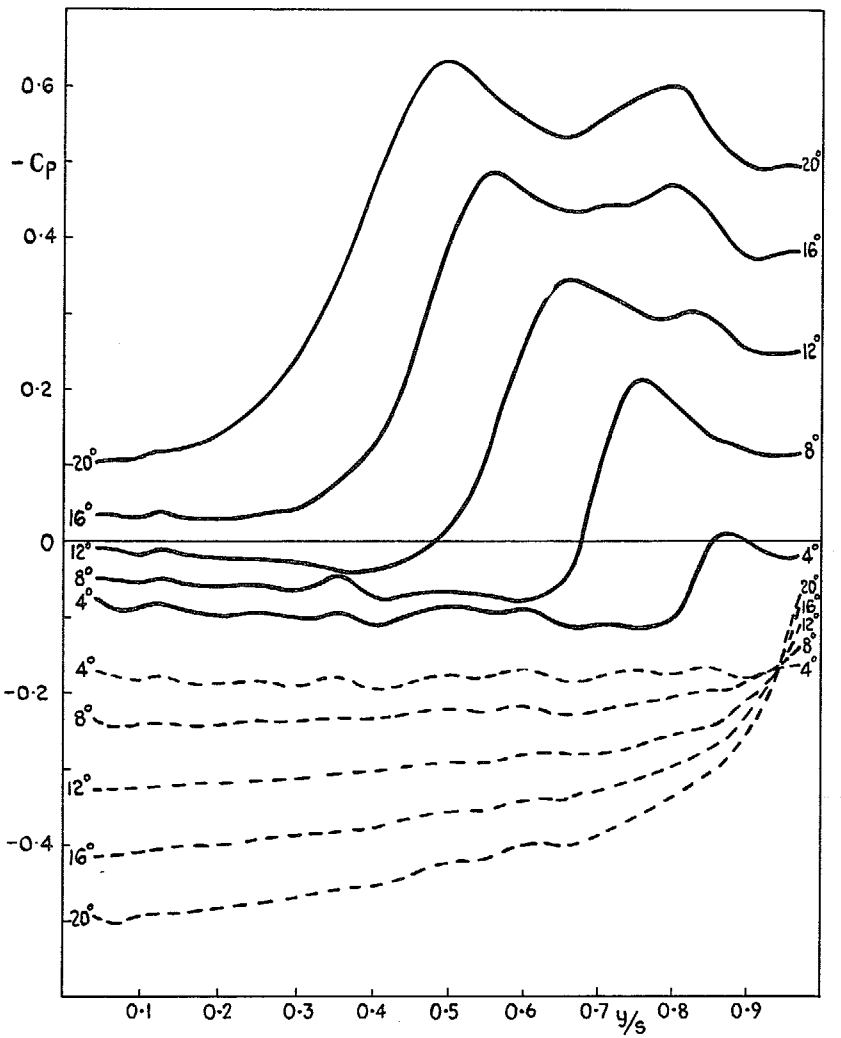

FIG. 5c. Pressure distributions at forward station, transition free, $M = 1$, various incidences.

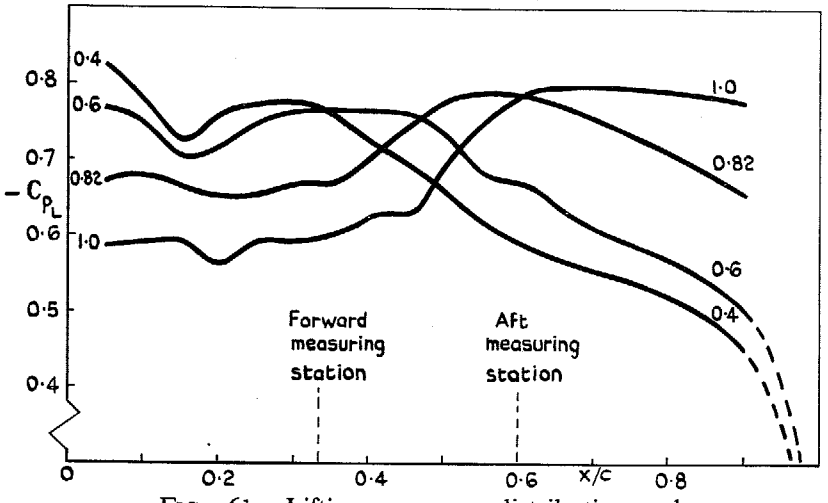

FIG. 6a. Lifting pressure distributions along generator, $\alpha = 16°$, transition free, various Mach numbers, upper surface.

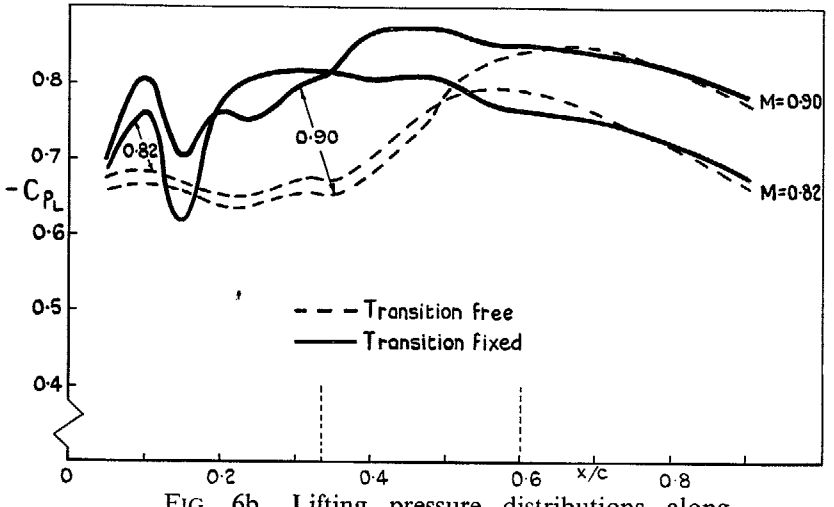

FIG. 6b. Lifting pressure distributions along generator, $\alpha = 16°$, $M = 0{\cdot}82$ & $0{\cdot}90$, transition free and fixed, upper surface.

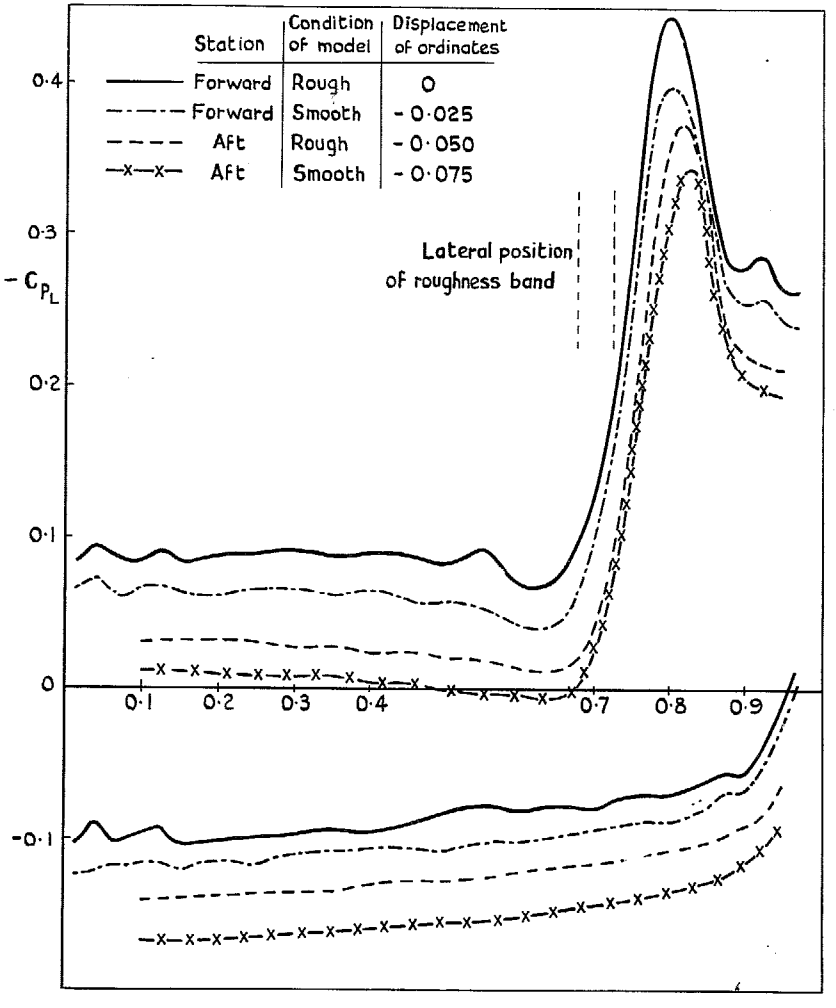

FIG. 7a. Lifting pressure distributions, $M = 0{\cdot}6$, $\alpha = 8°$.

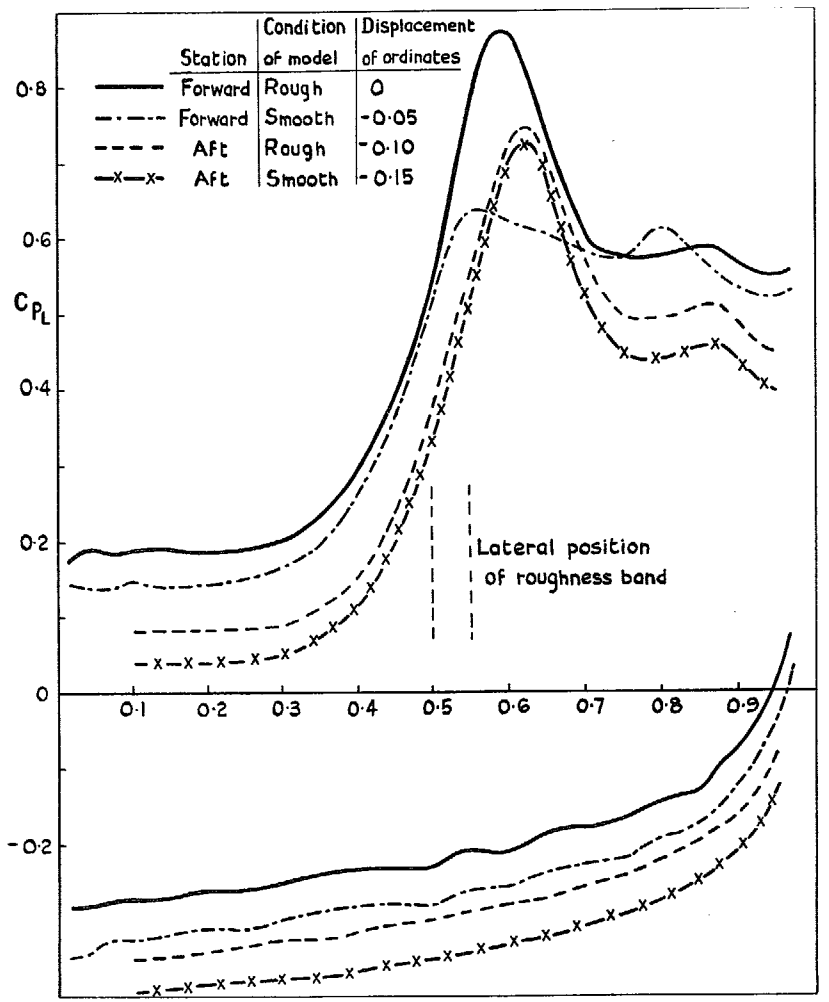

FIG. 7b. Lifting pressure distributions, $M = 0{\cdot}9$, $\alpha = 16°$.

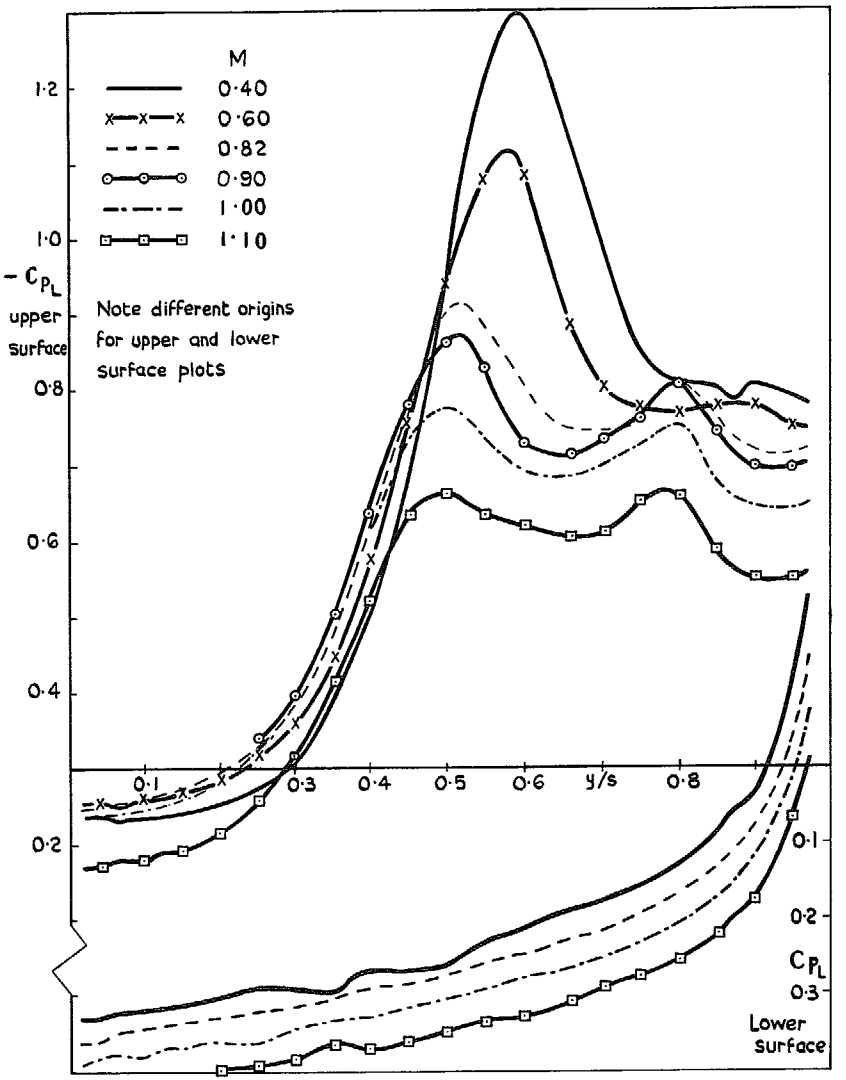

FIG. 8a. Lifting pressure distributions, forward station, transition free, $\alpha = 20°$.

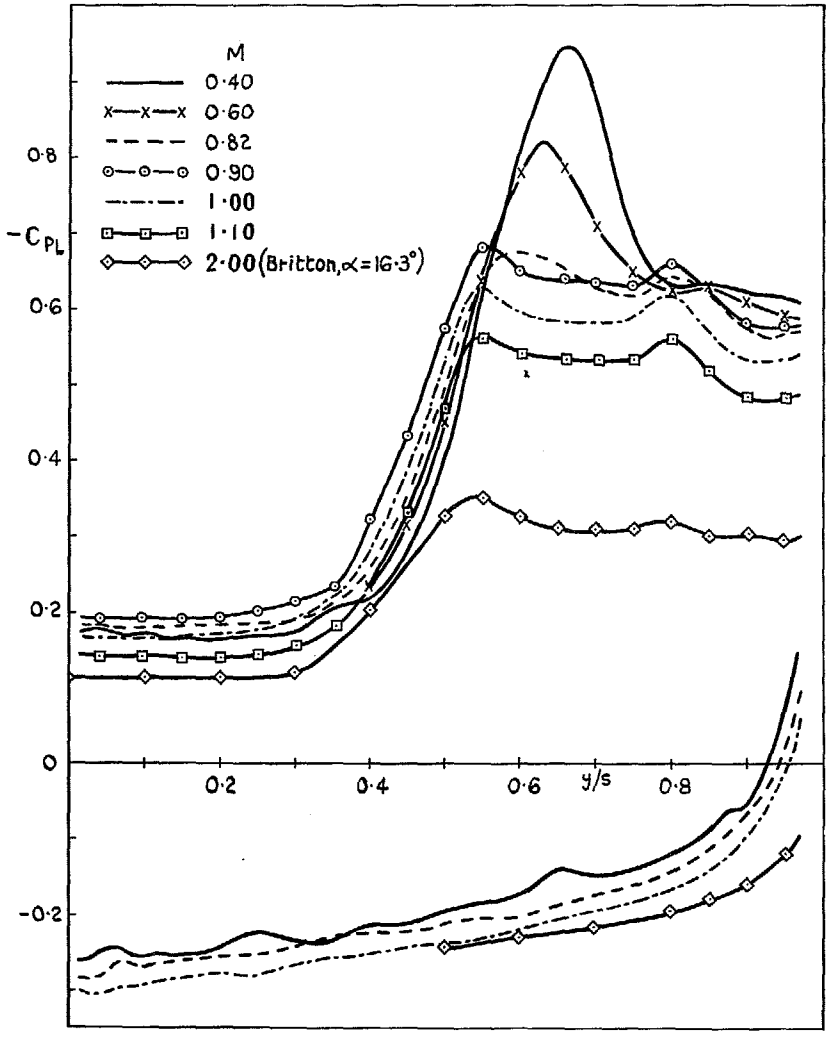

FIG. 8b. Lifting pressure distributions, forward station, transition free, $\alpha = 16°$.

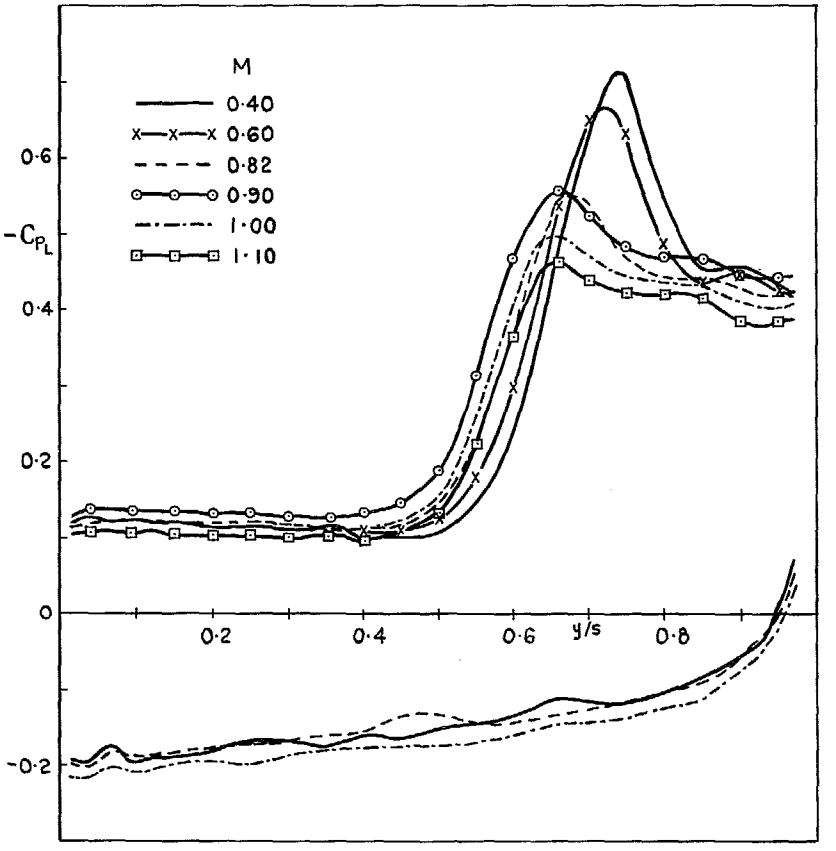

FIG. 8c. Lifting pressure distributions, forward station, transition free, $\alpha = 12°$.

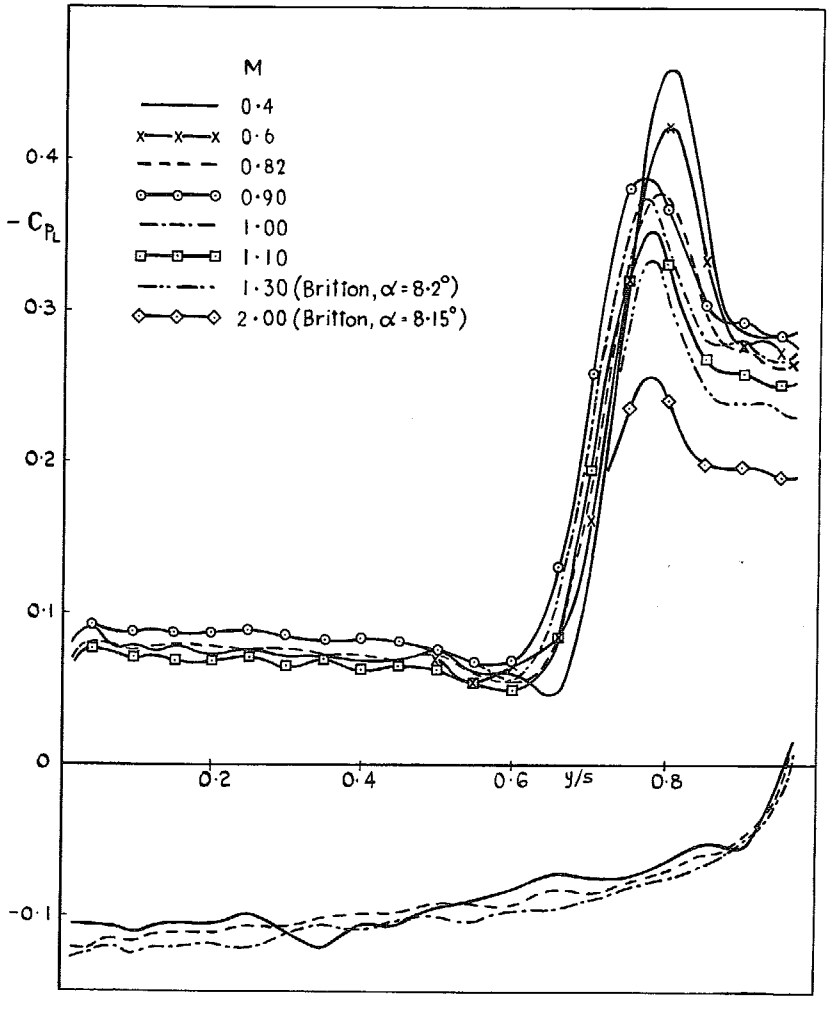

FIG. 8d. Lifting pressure distributions, forward station, transition free, $\alpha = 8°$.

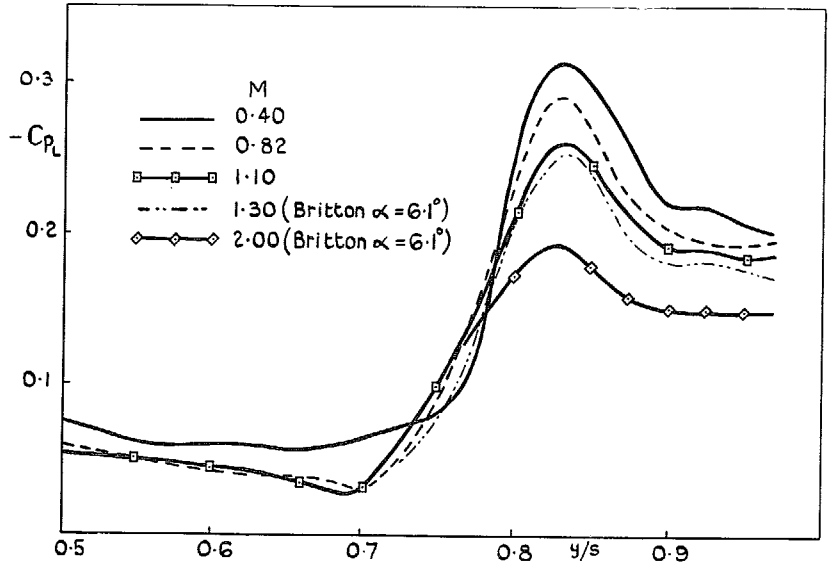

FIG. 8e. Lifting pressure distributions, forward station, transition free, $\alpha = 6°$.

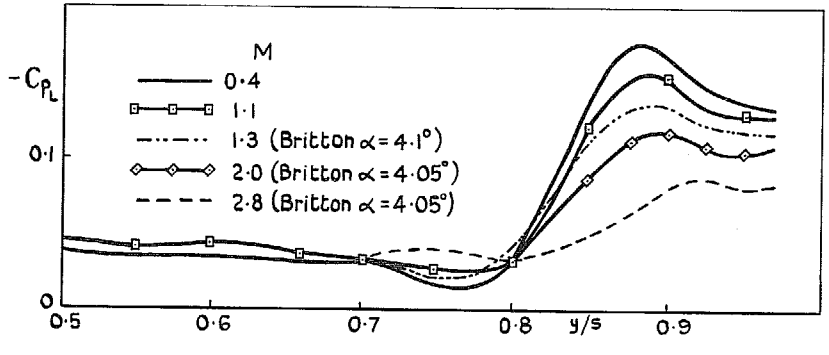

FIG. 8f. Lifting pressure distributions, forward station, transition free, $\alpha = 4°$.

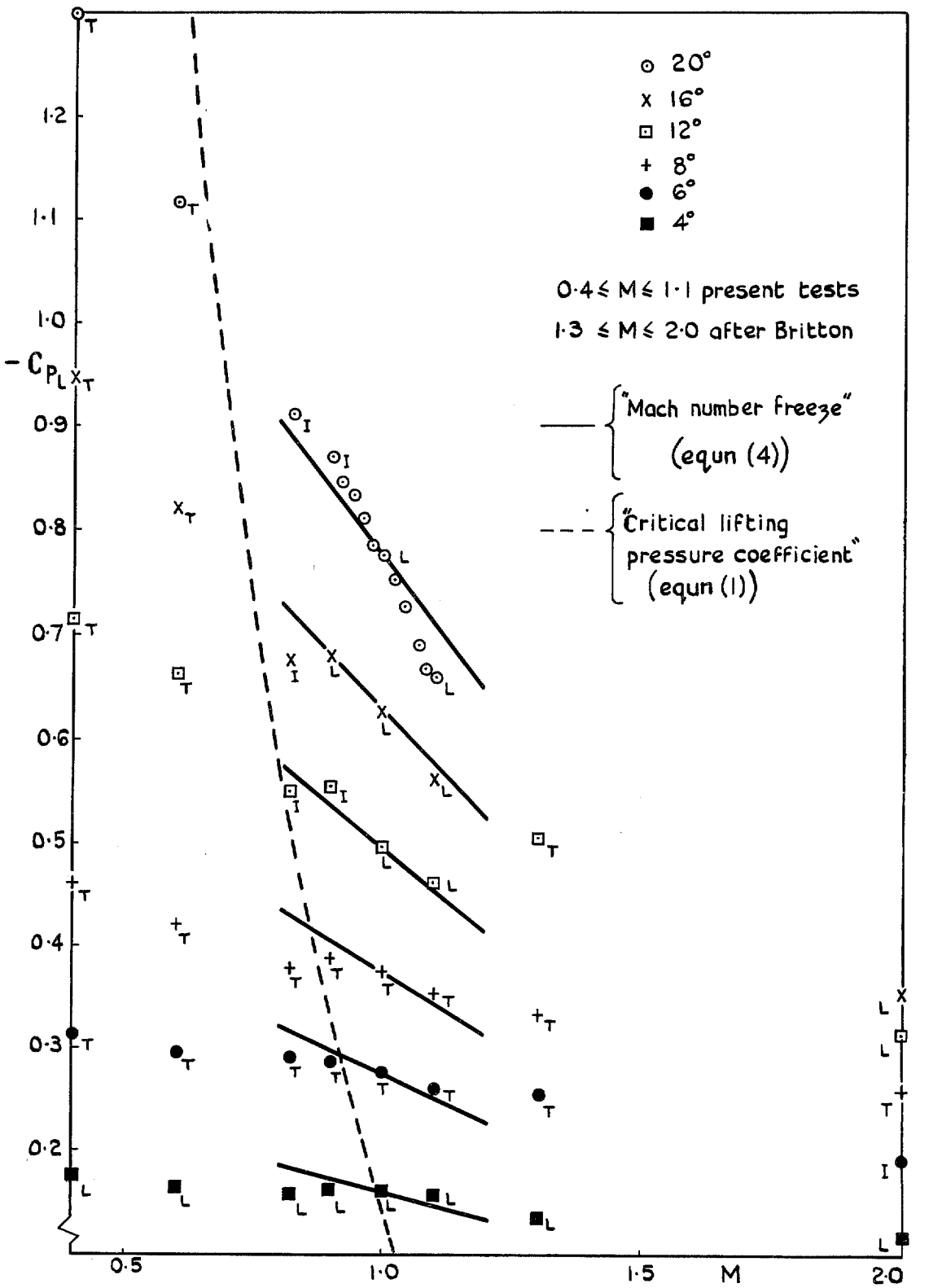

FIG. 9. Peak values of lifting pressure coefficient, transition free.

Printed in Wales for Her Majesty's Stationery Office by Allens Printers (Wales) Limited
Dd 146916 K5

Published by
HER MAJESTY'S STATIONERY OFFICE

To be purchased from
49 High Holborn, London WC1
13a Castle Street, Edinburgh EH2 3AR
109 St Mary Street, Cardiff CF1 1JW
Brazennose Street, Manchester M60 8AS
50 Fairfax Street, Bristol BS1 3DE
258 Broad Street, Birmingham 1
7 Linenhall Street, Belfast BT2 8AY
or through any bookseller

SBN 11 470326 4